Insights into the structure and dynamics of the upper mantle beneath Bass Strait, southeast Australia, using shear wave splitting

M. Bello[*1,2], D.G. Cornwell[1], N. Rawlinson[3] and A. M. Reading[4]

[1]School of Geosciences, University of Aberdeen, Aberdeen, UK
[2]Department of Physics, Abubakar Tafawa Balewa University, Bauchi, Nigeria
[3]Department of Earth Sciences-Bullard Labs, University of Cambridge, Cambridge, UK
[4]School of Natural Sciences (Physics), University of Tasmania, Tasmania, Australia

We investigate the structure of the upper mantle using teleseismic shear wave splitting measurements obtained at 32 broadband seismic stations located in Bass Strait and the surrounding region of southeast Australia. Our dataset includes ~366 individual splitting measurements from SKS and SKKS phases. The pattern of seismic anisotropy from shear wave splitting analysis beneath the study area is complex and does not always correlate with magnetic lineaments or current N-S absolute plate motion. In the eastern Lachlan Fold Belt, fast shear waves are polarized parallel to the structural trend (~N25E). Further south, fast shear wave polarization directions trend on average N25-75E from the Western Tasmania Terrane through Bass Strait to southern Victoria, which is consistent with the presence of an exotic Precambrian microcontinent in this region as previously postulated. Stations located on and around the Neogene-Quaternary Newer Volcanics Province in southern Victoria display sizeable delay times (~2.7 s). These values are among the largest in the world and hence require either an unusually large intrinsic anisotropy frozen within the lithosphere, or a contribution from both the lithospheric and asthenospheric mantle. In the Eastern Tasmania Terrane, nearly all observed fast directions are approximately NW-SE. Although part of our data set strongly favours anisotropy originating from "fabric" frozen in the lithospheric mantle, a contribution from the asthenospheric flow related to the present day plate motion is also required to explain the observed splitting parameters. We suggest that deviation of asthenospheric mantle flow around lithospheric roots could be occurring, and so variations in anisotropy related to mantle flow may be expected. Alternatively, the pattern of fast polarisation orientations observed around Bass Strait may be consistent with radial mantle flow associated with a plume linked to the recently discovered Cosgrove volcanic track. However, it is difficult to characterise the relative contributions to the observed splitting from the lithospheric vs. asthenospheric upper mantle due to poor backazimuthal coverage of the data.

KEY WORDS: mantle anisotropy, lithosphere, asthenosphere, shear-wave splitting, SKS/SKKS phases, southeast Australia

1. Introduction

The tectonic evolution of southeast Australia's Palaeozoic orogens (part of the eastern Australian Tasmanides) is yet to be fully understood, with most of the proposed models not in agreement with regard to the presence of entrained Precambrian continental fragments (Glen, 2005; Cayley et al., 2002; Cayley, 2011, Moresi et al., 2014; Pilia et al., 2015a; Pilia et al., 2015b; Pilia et al., 2016), geometry and number of subduction zones involved in the

accretionary process (Gray and Foster, 2004; Fergusson et al., 2009; Fergusson, 2014; Glen, 2014) and age and extent of metamorphism of the various tectonic blocks that form the orogens (Glen, 2005; Moore et al., 2013, Moore et al., 2015). Despite the lack of consensus, there appears little doubt that a complex sequence of events was required to build the Tasmanides, and the deformation processes involved would likely leave a clear signature of elastic wave anisotropy frozen into the lithosphere. Shear wave splitting measurements can be used to probe patterns of deformation at depth because it is an unambiguous indicator of seismic anisotropy and hence an essential tool in understanding the structure and dynamics of the Earth's deep interior (e.g. Vinnik et al., 1984; Silver and Chan, 1988; Long and Silver, 2009; Long and Becker, 2010).

In the upper mantle, seismic anisotropy results mainly from crystallographic or lattice preferred orientation (LPO) of intrinsically anisotropic mineral, primarily olivine. This is caused by deformation-induced alignment of the anisotropic minerals in the asthenosphere or past deformation of the lithosphere (e.g. Nicolas and Christensen, 1987; Silver and Chan, 1988; Zhang and Karato, 1995; Long and Becker, 2010; Mainprice et al., 2000). In addition to this, a contribution to anisotropy from shape-preferred orientation (SPO) might be present if materials with elastically distinct properties, such as melt lenses or fluid-filled microcracks, align preferentially (e.g. Silver, 1996; Silver and Chan, 1988). Some studies suggest that the alignment of fluid-filled microcracks in response to an applied stress field is a dominant cause of anisotropy in the crust (e.g. Crampin, 1987; Babuska and Cara, 1991; Crampin 1994). However, the tectonic fabric of continental regions that are subjected to strong deformation leads to lineations, foliations and other structures that develop in response to tectonic forces, and may be preserved in the crust as strain-induced mineral alignment (LPO or SPO).

When a seismic shear wave passes through an anisotropic medium, it splits into two orthogonal quasi-shear waves, one travelling faster than the other with a time lag (δt) which is observed between the "fast" and "slow" polarised shear waves when they arrive at the receiver (e.g. Silver, 1996). One of the two waves is also orientated parallel to the direction (φ) of the anisotropy, and the other is orientated perpendicular. The size of the time lag depends on the thickness of the anisotropic layer and/or the intensity of anisotropy. The time

lag between the fast and slow components results in non-zero energy on the tangential-component seismogram and an elliptical particle motion. The fast-polarization orientation (φ) and time delay (δt) parameters provide simple measurements that characterize the seismic anisotropy of the medium (e.g. Silver and Chan, 1991).

The splitting parameters can be related to preserved/fossil anisotropy frozen in the lithosphere (e.g. Vauchez and Nicolas, 1991; Bastow et al., 2007), present-day sub-lithospheric flow which is principally controlled by plate motion (e.g. Vinnik et al., 1992; Fouch et al., 2000; Sleep et al., 2002), the preferential orientation of fluid or melt bodies (e.g. Blackman and Kendall, 1997), or combinations of these factors. Seismic arrivals such as SKS, PKS, and SKKS are the most suitable phases for shear wave splitting studies of the lithosphere beneath a seismic station because they involve P-to-S conversions at the core-mantle boundary. Hence, no source side anisotropy is preserved, and these phases are horizontally polarized on exiting the core-mantle boundary (e.g. Savage, 1999). The near-vertical incidence of the arrivals also results in good lateral resolution of <50 km if a dense array of seismometers is deployed (Savage, 1999).

The aim of this study is to use seismic anisotropy derived from shear wave splitting to provide insights into the lithospheric structure and possible mechanical coupling between the crust and the upper mantle beneath Bass Strait and adjoining landmasses. Data in this case is supplied by temporary and permanent arrays of broadband seismometers that span southeastern New South Wales, southern Victoria, Bass Strait and Tasmania. The study also aims to provide insight into the tectonic relationship between different tectonic blocks in the southern part of the Tasmanides.

2. Tectonic setting

At the onset of the Phanerozoic, the Australian continent witnessed a new phase of tectonic evolution dominated by subduction related accretion, which added nearly one third of the present day continental lithosphere to the eastern margin (Betts et al., 2002). The so-called Tasman Orogen or “Tasmanides” are a series of orogenic belts that have developed along the margin of eastern Australia from the Cambrian to the Triassic (Foster and Gray, 2000; Glen,

2005). These orogenic belts have an approximate NE-SW dominant structural trend and comprise the Delamerian, Lachlan, Thomson and New England Orogens (Fig. 1).

On mainland Australia, the oldest orogeny in the Tasmanides is the Delamerian Orogeny (Fig. 1). It began during the Middle Cambrian with convergence along the proto-Pacific margin of East Gondwana and culminated in a foreland style fold and thrust belt which featured high-temperature, low-pressure metamorphism associated with intrusive magmatism (Betts et al., 2002). A number of studies (e.g. Reed et al., 2002; Crawford et al., 2003) suggest that the Delamerian Orogen extends southwards from mainland Australia into western Tasmania, where it is referred to as the Tyennan Orogen. This connection is reinforced by several studies which examined the age and geochemistry of various igneous rocks in both regions, and found strong similarities (e.g. Direen and Crawford, 2003).

Adjoining the Delamerian Orogen to the east is the Lachlan Orogen whose evolution is thought to have begun in the Late Cambrian and was largely complete by the Middle to Late Devonian. The Lachlan Orogen is well known for its complex tectonic history that includes several orogenic episodes that are recorded in the rock record as a series of distinct deformational events (Gray and Foster, 2004; Glen, 2005). Previous studies (e.g. Gray and Foster, 2004) have argued for a tectonic model that involved interaction of oceanic microplates, a volcanic arc, multiple turbidite-dominated thrust systems and three major subduction zones within the Lachlan Orogen. Each of the subduction zones is associated with accretion of discrete terrains, namely the Stawell-Bendigo zones of western Victoria, the Tabbarebera zone of eastern Victoria and the Narooma accretionary complex along the east coast (Fig. 1). The evolution of the Lachlan Orogen is yet to be fully understood because of the complexity of the surface geology, the limited exposure due to the presence of Mesozoic and Cenozoic sedimentary basins and Quaternary volcanics which obscure a large proportion of the Palaeozoic terrane, and a limited knowledge of the deep structure and composition of the lithosphere.

The relationship between the Lachlan Orogen and Thomson Orogen, which lies to its North, has traditionally been difficult to determine largely because of extensive sedimentary cover from the Mesozoic Murray and Eromanga basins (Fig. 1)(Glen et al., 2013; Burton and

Trigg, 2014; Glen et al., 2014). However, recent geophysical and geochemical studies (Siegel et al., 2018; Spampinato et al., 2015) have suggested that the Thompson Orogen is floored with Precambrian continental crust, which is in contrast to the Palaeozoic oceanic substrate of the Lachlan Orogen. To the northeast of the Lachlan Orogen is the New England Orogen, which formed between the Late Devonian and Triassic and is the youngest fold belt in the Tasmanides. The New England Orogen formed as an east facing convergent margin Orogen (Glen, 2005; Rosenbaum et al., 2012) and although there is some evidence of a shared Cambrian history between the New England and Lachlan Orogens (Glen, 2013), this relationship is obscured by the presence of post emplacement sedimentary cover of the Permian to Triassic Sydney Basin.

Significant tectonic events that have shaped southeast Australia subsequent to the formation of the Tasmanides include the break up of Australia and Antarctica, and the opening of the Tasman Sea and Bass Strait around 80-90 Ma (Gaina et al., 1998). These events resulted in lithospheric thinning towards the passive margin and failed rifting in Bass Strait led to the formation of three intracratonic rift basins (Bass, Gippsland and Otway). These basins largely accommodate Cretaceous to Quaternary sediments (Lister et al., 1991; van der Beek et al., 1999).

In a recent study, it was shown that the Cosgrove volcanic track traversed almost the entire eastern seaboard of Australia (Davies et al., 2015), with its last known eruptions likely associated with the Quaternary Newer Volcanics province in western Victoria between ~4.5 Ma and 5 kyr ago (Rawlinson et al., 2017). The current location of the underlying plume – if it still exists – is roughly beneath the centre of Bass Strait (Davies et al., 2015), where a regional surface wave tomography study indicates the presence of a low velocity zone to depths of ~150 km (Fishwick and Rawlinson, 2012).

South of Bass Strait, Tasmania largely comprised what is now referred to as the West Tasmania Terrane in the Early to Middle Phanerozoic (Fig. 1)(Black et al., 2004). The evolution of this region began as long ago as 800–750 Ma (Turner et al., 1998), with pervasive granite emplacement on King Island and deposition of thick turbidite sediments in NW Tasmania. The major event that shaped western Tasmania was the Middle to Late

Cambrian Tyennan Orogeny, which was a period of significant deformation (Elliot et al., 1993). Several models have been proposed to explain the origin of the Tyennan Orogeny, which range from westerly subduction to easterly subduction to even a purely extensional regime in which the felsic Mount Read Volcanic arc formed as a result of rifting (Corbett et al., 1972). More recent models suggest that an east–facing Tasmanian passive margin collided with an oceanic arc in the Early to Middle Cambrian, resulting in obduction of mafic-ultramafic complexes across much of Tasmania (Berry and Crawford, 1988; Crawford and Berry, 1992; Turner et al., 1998). In a possible second stage of the obduction process, fault bounded Proterozoic units displaying anomalous high-grade metamorphism are also thought to have been emplaced (Berry, 1995; Maffre et al., 2000; Holm and Berry, 2002; Berry et al., 2007).

On the other hand, the East Tasmania Terrane (Fig. 1) contains no evidence of the Tyennan Orogeny or Proterozoic outcrop, and it is widely thought that the two terranes were sutured together during the Middle Devonian Tabberabberan Orogeny (Elliot et al., 1993). Differences in stratigraphy across the so-called Tamar Fracture System in northern Tasmania (Fig. 1) motivated several workers to suggest that the fracture zone represents the crustal-scale suture between the East and West Tasmania terranes (Williams, 1989). The stratigraphy exhibits Proterozoic sedimentary and Palaeozoic volcanic and sedimentary successions in the west, while a thick sequence of Lower to Middle Palaeozoic turbidites lie to the east (Reed, 2001). However, south of the Tamar Valley, widespread late Carboniferous sedimentary deposits and Jurassic dolerite sheets conceal any evidence of a crustal scale suture zone. In addition, potential field data (Leaman, 1994) do not support the existence of a major terrane boundary beneath the inferred Tamar Fracture System.

In an effort to link Tasmania and mainland Australia many models have been proposed. Although these models are often in conflict, one model that has recently gained widespread support is the Selwyn Block model of Cayley et al. (2002). Using evidence from potential field and outcrop data, Cayley et al. (2002) suggested that a Precambrian fragment of continental crust is embedded within the Tasmanides, which they termed the “Selwyn Block”. The western part of Bass Strait features strong magnetic lineaments that can be traced without major disruption from northwestern Tasmania to Victoria, which is seen as

one of the primary pieces of supporting evidence for its presence. In a subsequent study, Cayley (2011) proposed a new tectonic model of southeast Australia, which involves a Proterozoic exotic microcontinent termed “VanDieland”. The microcontinent VanDieland comprises the Selwyn Block, West Tasmania Terrane and the surrounding western region of Bass Strait. This fragment, postulated to be of Rodinia origin, was embedded in a convergent accretionary margin during proto-Pacific subduction along eastern Australia. In a more recent paper, Moresi et al. (2014) suggested that the entrained microcontinent caused the formation of a large orocline that underlies the Lachlan Orogen. This occurs as a result of a complex sequence of processes including differential roll back and southward transfer of material through an extensive continental transform fault. This scenario is consistent with the model of Cayley et al. (2011).

3. Previous geophysical studies

In addition to studies which focus on geological similarities, potential field data and geodynamic modelling, other geophysical observations have been used to help discriminate between the different tectonic models that have been proposed. For example, several seismic tomography models for southeast Australia that have recently been published provide an unprecedented level of detail on crust and upper mantle structure beneath the region (e.g., Graeber et al., 2002; Rawlinson et al., 2006; Rawlinson and Urvoy 2006; Rawlinson and Kennett, 2008; Rawlinson and Fishwick, 2011; Rawlinson et al., 2015; Pilia et al., 2015a; Pilia et al., 2015b; Pilia et al., 2016; Rawlinson et al., 2016). In particular, Pilia et al., (2015a) used ambient noise tomography to image several striking structural features in the mid-lower crust beneath southeast Australia, including a NW-SE high velocity anomaly that is interpreted to be the Proterozoic connection between north-western Tasmania and south-central Victoria. This model also reveals three pronounced north-south high velocity belts that appear to span Bass Strait with little evidence of interruption from more recent tectonic events.

Studies carried out by Debayle and Kennett (1998), Debayle (1999) and others using surface wave tomography, which incorporates azimuthal anisotropy, suggested a two-layer system of anisotropy beneath Australia: in the upper layer, directions of anisotropy are

approximately oriented east–west in Debayle (1999), but more or less randomly in Simons and van der Hilst (2003). In the bottom layer, directions of anisotropy appear to be north–south, approximately parallel to absolute plate motion (APM) (Gripps and Gordon, 2002) in both models. In a more recent study, Pilia et al. (2016) related crustal azimuthal anisotropy to regional tectonics using ambient noise tomography. Their study indicated that the directions of crustal anisotropy are approximately north–south beneath mainland southeast Australia, and approximately east-west in Bass Strait and Tasmania. This result is used to carry out a comparative analysis with our results in the discussion section.

Seismic anisotropy beneath the study area has also been examined (albeit at much lower spatial resolution) through measurements of SKS/SKKS splitting for over 20 years (e.g., Vinnik et al., 1992; Girardin and Farra, 1998; Clitheroe and van der Hilst, 1998; Ozalaybey and Chen, 1999; Barruol and Hoffman, 1999; Eaton et al., 2004; Heintz and Kennett, 2005; Frederiksen et al., 2007). Of particular importance here is the study of Heintz and Kennett (2005), who used a continent wide network of 190 temporary stations with an average recording span of 6 months, which is rather limited for SWS analysis. However, the results show a complex pattern of anisotropy, which does not correlate with the contemporary plate motion direction of Argus et al. (2002). Despite the limited data availability and limited geological outcrop, especially in Phanerozoic southeast Australia which is almost entirely covered by sedimentary basins, a number of relationships were highlighted between fast polarization directions and structural trends. These relationships were interpreted to arise from anisotropy frozen into the lithosphere as a result of regional deformation events. Barruol and Hoffman (1999) studied upper mantle anisotropy using GEOSCOPE stations and attempted to explain the apparent isotropy at station “CAN”. Their study was the first to suggest an E-W anisotropic layer overlying a N-S anisotropic layer at this station. Clitheroe and van der Hilst (1998) investigated the variation in shear wave splitting across the Australian continent and showed that differing SKS splitting phenomena manifest at different frequencies, with shear wave splitting only observed at frequencies higher than 0.3 Hz. From the splitting measurements of only two stations in the neighbourhood of Tasmania, Bass Strait and adjoining southern Victoria, in which one station recorded scant S core phases and the other yielded abundant nulls, they concluded that splitting measurements in this region are either ambiguous or not well constrained.

In this paper, we present new shear wave splitting measurements across southeast Australia from both permanent seismograph stations and a recent network of temporary stations, covering a region that spans Proterozoic and Palaeozoic lithosphere. This significantly larger number of stations allows us to examine shear wave splitting variations in much more detail than has previously been possible, thus allowing us to make new inferences about the anisotropic nature of the crust and upper mantle in this region of the Tasmanides.

4. Data and methods

This study utilises seismological data from a network of 24 temporary stations that recorded for approximately 23 months (22/05/2011 to 28/04/2013) and eight permanent stations of which six are maintained by the Australian National Seismic Network (ANSN) and the remaining two are each maintained by IRIS and GEOSCOPE. The temporary stations consist of 23 Güralp 40T three-component broadband seismic stations and one Güralp CMG-3ESP broadband sensor that together span southern Victoria, several islands in Bass Strait (i.e. Flinders, King and Deal Islands) and northern Tasmania (Fig. 2). The average spacing of the temporary stations is ~80–120 km. The GSN permanent station maintained by IRIS named TAU is located in Hobart, Tasmania and has been running for ~23 years (1994-2017), while the GEOSCOPE station named CAN is located in Canberra, in mainland Australia and has been in operation since 1987 (~30 years). The six ANSN permanent stations that have been running for ~13 years are spread between Young in New South Wales and the highlands of Tasmania (Fig. 2).

We extracted data corresponding to earthquakes within epicentral distances of 85° to 140° from the centre of the network; this distance criterion is necessary to separate core S phases (SKS and SKKS) from non-radially polarized phases such as S and ScS. Visual inspection revealed that events with $M_w \geq 6.0$ provided the best signal to noise ratio and waveform clarity. Based on this, earthquakes with magnitude $M_w \geq 6.0$ were selected from the global ISC catalogue for permanent stations (Fig. 3). However, due to the shorter recording duration of the temporary stations, data from carefully selected earthquakes with magnitude $M_w \geq 5.5$ within the same epicentral distance range were also extracted for analysis.

As part of basic data pre-processing, we filtered the seismograms between 0.03 and 0.5 Hz, using a two-pole, two-pass Butterworth band-pass filter. The quality of the data was further inspected and only traces showing sharp arrivals of core phases, which are very distinct from the surrounding noise, were retained for analysis (Fig. 4).

Shear wave splitting measurements were performed on core refracted shear waves using the method of Teanby et al., (2004), which is based on the approach of Silver and Chan, (1991). Horizontal-component seismograms were rotated, with one component time shifted to minimize the second eigenvalue of the particle motion in the analysis window, thus linearising particle motion. A grid search over plausible values of φ and δt (with respective increments of 1° and 0.05 s) was performed to find the optimum solution that best removes the influence of anisotropy. A measurement window was manually picked (~10 s before SKS/SKKS arrival and ~10 s after) and individual measurements were made between the start and end time of the window. Using measurements over a set of 100 windows around the SKS or SKKS arrival, cluster analysis was then used to identify the most stable splitting parameters φ and δt corresponding to the measurement with the smallest errors.

SKS splitting results generally fall into two categories. A split wave that passes through an anisotropic medium initially shows significant energy on the tangential component and an elliptical particle motion. When the seismograms are corrected for the optimum δt and φ, the waveforms will match, the tangential component energy is minimised, and the particle motion is linearised (Fig. 5). If the seismic wave passes through azimuthally isotropic material, or if its azimuth (source polarisation) is orientated parallel or perpendicular to the fast axis of anisotropy, or if multiple layers (complex anisotropy) of anisotropy cancel out, a characteristic “null” result will be observed (Fig. 6) (e.g. Barruol and Hoffmann, 1999). In this case, there will be no energy on the tangential component prior to correction, and the uncorrected particle motion will be linear.

A single pair of splitting parameters (δt and φ) can characterise a single, horizontal and homogeneous layer of anisotropy. The presence of more complex structure, such as two or more anisotropic layers, may be indicated by systematic variations with earthquake backazimuth (Levin et al., 1999). We examined the backazimuthal coverage for SKS/SKKS

phases in the study area and noted that it is not ideal, because it is heavily weighted towards events to the north and southeast of Bass Strait, which precludes a complete analysis of backazimuthal dependence of splitting parameters; this is shown in an event map (Fig. 3). Since the dataset contains this restriction, the presence of multiple anisotropic layers cannot be reliably inferred.

5. Results

We categorise individual shear wave splitting results based on: (1) the quality of the initial signal; (2) a clear separation between the fast and slow shear wave before transverse energy minimisation; (3) the ellipticity of the particle motion in the horizontal plane before transverse energy minimisation; (4) the linearisation of particle motion after transverse energy minimisation; and (5) the waveform coherence between the fast and slow split shear waves. We identified "good" measurements as those that satisfy the following criteria: (i) high waveform clarity; (ii) elliptical initial particle motion and linear or nearly linear particle motion after correction; (iii) splitting parameter estimates that were consistent within error along with fairly small error ellipses; and (iv) with errors less than ±10° in the fast direction and ± 0.20s in delay time. Measurements meeting only three criteria with larger error bars (up to ± 20° in φ and ± 0.30s in δt) and lower waveform clarity were marked as "fair". A poor measurement only fulfils two criteria and null measurements were identified by an initial linear particle motion and a lack of energy on the transverse component associated with the arrival of the core phase of interest on the radial component. An example of high-quality splitting and null measurements are shown in Figure 5 and 6, respectively.

After applying the splitting measurement procedure described in the previous section, a total of ~366 well-constrained measurements of φ and δt at 24 temporary and 8 permanent stations were obtained. Out of these, ~51 were classified as "good" and ~109 as "fair" In addition to these, ~206 high-quality ("good"+"fair") null measurements were identified. Some individual stations had 4–8 "good" quality measurements, while others had ≤3. At several stations the measurement procedure only yielded "fair" quality measurements and in some cases only "null" measurements were produced. This modest return of good results is consistent with previous shear wave splitting studies in the region.

The shear wave splitting parameter measurements (Fig. 7) were generally found to cluster relatively tightly around certain dominant directions. For this reason, despite long recording times at some of the stations, the measurements are largely confined to two or three relatively restricted back azimuthal ranges (Fig. 7). As noted earlier, the large gaps in azimuthal coverage do not allow for a direct interpretation of multi-layered anisotropic characteristics; therefore, we restrict our quantitative analyses to comparisons with the dominant anisotropic directions inferred from the full sets of measurements. A notable exception is station CAN in the northeastern part of the study area. The back azimuthal coverage here is slightly better than average, but almost two-thirds of the measurements indicate null results.

In order to present a clear first-order picture of SKS splitting patterns beneath the study area, we took a weighted mean of splitting parameters (φ, δt) for each station (Fig. 8)(splitting parameters can be found in the supplementary data). This represents an average value that weighs each individual non-null measurement by its value of φ and δt error bars. Good splits that generally have smaller error bounds are given more weight so that they contribute to the weighted mean more than fair splits. For the fast polarisation, this is done by averaging angles of the whole set of measurements (good and fair) as points on a unit circle in a Cartesian plane and then converting it back. The weighted means of splitting parameter values can be found in Table 1, with a plot of the resulting splitting orientations and delay times, and a histogram station performance indicated by the number of measurements at individual stations, shown in Figures 8 and 9 respectively.

There are some regional trends that are evident from Figure 8. First, the dominant splitting orientations range from NE-SW to NW-SE within a broadly N-S average. We note significant changes in splitting orientation between individual stations spaced ~300 to 500 km apart. Delay times are also highly variable, ranging from the smallest δt in Bass Strait of ~0.66±0.10s (BA01) to the largest δt in southern Victoria of ~2.70±0.25s (BA18). Despite the spatial variability in fast direction and delay time, some correlation can still be seen when looking at the results more closely, especially in: (1) the Lachlan Fold Belt (Eastern Lachlan Orogen); (2) the postulated micro-continent VanDieland; (3) East Tasmania Terrane (ETT) and Furneaux Islands; and (4) the Newer Volcanics Province.

In the Lachlan Fold Belt (Fig. 8), moderate to large delay times occur over the range 0.73±0.13 s (CNB) to 2.47±0.25 s (BA12) with a dominant approximate fast direction of NNE-SSW. These fast directions are sub-parallel to the structural trend of the Lachlan Fold Belt. One station of note here (CAN), which will be discussed in more detail later, has unusual splitting parameters. At this station, only fair measurements have been observed and the overall splitting measurement comprises abundant nulls from all backazimuths. In VanDieland there is a broad NE-SW variation in the fast direction from southern Victoria to western Tasmania. It is observed that stations in southern Victoria exhibit significant shear wave splitting, with average delay times at individual stations between ~1.15±0.24 s (BA21) and ~2.70±0.25 s (BA18) and an approximate fast direction of N-S to NE-SW. At the Bass Strait islands that form part of VanDieland, delay times are comparatively small (~0.66±0.10 s (BA01) to ~1.43±0.08 s (BA10)), with fast directions oriented in a roughly NE-SW direction. At the southern end of the micro-continent (western Tasmania), all observed fast directions are approximately NE-SW while the delay time is in the range ~0.74±0.13 s (BA02) to ~1.68±0.21 s (BA04). Looking at stations in the centre of southern Tasmania (MOO and TAU), the splitting measurements are in the range ~1.67±0.22 s (MOO) to ~2.07±0.43 s (TAU) and fast direction orientation is also approximately NE-SW.

The observed fast shear wave splitting directions for the East Tasmania Terrane (ETT) and Furneaux Islands show that the fast directions rotate from NW-SE in the East Tasmania Terrane (BA05, BA06) to E-W in the Furneaux Islands (BA07, BA08, BA09) and a delay time range of ~0.68±0.05 s to ~2.14±0.32 s is observed. Interestingly, the concentration of large delay times delineates a region in the heart of the Newer Volcanics Province (NVP) (Fig. 8). Some stations surrounding the NVP exhibit somewhat larger delay times than more distant stations.

The splitting pattern shown in Figure 8 is largely consistent with results from previous studies of shear wave splitting in south east Australia (e.g., Heintz and Kennett, 2005), although the data set described here has a much longer recording duration and spatial resolution. The pattern of fast directions found in our study region is also generally consistent with the larger-scale splitting pattern observed across the Australian continent (e.g., Clitheroe and van der Hilst, 1998; Heintz and Kennett, 2005; Barruol and Hoffman,

1999).

6. Discussion

The main challenge in studying core-refracted shear waves is the lack of vertical resolution due to near vertical paths of the SKS/SKKS phase through the upper mantle. The anisotropy measured at the surface has been acquired between the core-mantle boundary (CMB) and the surface; the splitting parameters therefore represent a path-integrated measurement and a key question is whether the splitting observed in the study area reflects anisotropy in the crust, in the mantle lithosphere (reflecting past deformational episodes), in the asthenosphere (related to present-day mantle flow), or a combination of these factors. If we consider an asthenospheric source of anisotropy, the mantle flow can be of two types: passive (Couette flow) and active (Poiseulle flow) (Stotz et al., 2017, 2018). Couette flow is generated in the asthenosphere by overlying plate motion; the associated horizontal shear stresses cause asthenospheric deformation beneath the plate. On the other hand, Poiseulle flow is driven by internal forces (pressure gradient) within the asthenosphere, such that flow velocities peak in the middle of the asthenospheric channel. Studies show that these two forces can occur together and any asthenospheric flow pattern is a linear combination of Couette and Poiseulle flow pattern (Stotz et al., 2018). If the source of the observed anisotropy is considered to be the asthenospheric flow, then this can lead to coherent splitting parameters over scale lengths >600 km (Becker et al., 2007). In this situation, the orientation of the polarisation plane of the fast shear wave would be parallel to the Absolute Plate Motion (APM) direction (Tommasi, 1998). However, our results neither indicate very coherent splitting parameters over large regions nor alignment of fast shear wave with APM direction. This will be investigated in more detail below.

6.1 Implications for plate tectonic evolution in SE Australia

At stations located in the Lachlan Fold Belt (CNB, CAN, BA12, BA13, BA14, BA15, BA16, BA19, DLN, YNG), the relative contributions to the observed splitting from the crust, mantle lithosphere, and asthenosphere are difficult to characterise due to poor

backazimuthal coverage of the data. However, the direction of anisotropy is parallel to the structural trend of the Lachlan Fold Belt i.e. NE-SW (Stations BA12, BA14, BA15, BA16 CNB, DLN, YNG). These measurements may be caused by fossil anisotropy in the lithosphere sourced from deformation-induced alignment of minerals related to the formation of the Palaeozoic Lachlan Fold Belt. However, we note that at 145°E and 38°S, the plate motion is approximately 59 mm/yr in the direction N20°E (estimated from NNR-MORVEL56 – see Argus et al., 2011), which means that a significant contribution from the sublithospheric mantle cannot be ruled out. Measurements performed at CNB are similar to those obtained by Clitheroe and Van der Hilst (1998), accounting for a weighted mean average of δt=1.40±0.06s and φ=38±6° that coincides with the NE-SW trend of the Lachlan Fold Belt.

At GEOSCOPE station CAN, clear evidence was found for either NE-SW or NW-SE oriented φ. These findings are consistent with a two-layer model, as suggested by Barruol and Hoffmann (1999), in which the two layers have roughly similar δt and anisotropy in each layer has a perpendicular orientation with respect to the adjacent layer. The anisotropic φ of the lower layer is roughly parallel (approximately northward) to the current plate motion direction. This model is supported by results from surface wave tomographic studies (e.g. Debayle and Kennett, 2000), which reported a change in anisotropic pattern at approximately 150 km depth. Moreover, in another study focussing on this particular station, Girardin and Farra (1998) suggested a two-layer model, where the 140 km upper layer has a roughly EW oriented φ and a 40 km thick lower layer with a N-S φ parallel to the current plate motion direction. CAN also has abundant and good back-azimuthal coverage of nulls, indicating either the absence of anisotropy along the ray path or that the fast polarisation is orthogonal to the direction of anisotropy (Fig. 10). Silver and Savage (1994) pointed out that apparent isotropy may be consistent with a simple two-layer model, where the two layers exhibit the same intrinsic and mutually perpendicular fast directions. Here, the medium may either be isotropic or the initial polarisation is parallel to the fast or slow direction of anisotropy for that propagation direction. Although the structure at station CAN is illuminated by a relatively better backazimuthal coverage, shear wave splitting observations suggest dominance of usable events arriving at a backazimuth around N0-N30°E and N120-N180°E. This station also exhibits a significant variation in both delay

time and fast polarisation direction with backazimuth and well constrained nulls were identified over a large swath of backazimuths; such a pattern is consistent with complex anisotropic structure beneath a station (e.g. Silver and Savage, 1994). In an ideal case of a simple, horizontal two-layered structure the apparent anisotropy parameters should vary with a $\pi/2$ periodicity. This is not the case with the station CAN and all other stations within the Lachlan Orogen; hence other factors like dipping structures or lateral heterogeneity may be present. Overall, splitting patterns at individual stations in this region are often complicated, which implies that the anisotropic structure beneath this region is also complex. This reinforces a likely contribution from several different regions of the crust and/or upper mantle that augment or cancel each other out.

Elsewhere on mainland Australia in our study region, there are three stations (BA23, BA24 and MILA) where no reliable measurements have been found except for several coherent null measurements. Whether this is a true reflection of anisotropic structure in this region is difficult to tell because these stations are generally characterised by poor quality data.

The splitting pattern in the microcontinent (VanDieland) can be divided into two groups: (1) Western Tasmania Terrane (WTT); and (2) the Selwyn Block (the northward extension of west Tasmania that spans Bass Strait and penetrates beneath central Victoria) and submerged continental crust adjacent to Tasmania. In the WTT, stations BA01, BA02, BA03 have a NE-SW direction of fast polarisation that ranges from 38±3° to 65±3°. The stations highlight some correlation between fast shear wave polarisation directions and the trend of the dominant surface structures; however, it shows a poor correlation with APM (~N20°E) and thus asthenospheric flow, while it could be one of the main causes, cannot be considered as the principal cause of the observed anisotropy. These stations (WTT) and the stations in the northeast of Tasmania (ETT) (BA04, BA05, BA06) have similar attributes in terms of correlation between fast shear wave polarisation direction and the trend of dominant surface structures as well as poor correlation with APM except that the dominant fast polarisation direction north east of Tasmania (ETT) is NW-SE (-48±3° to -86±4°). Our mean splitting measurement from the permanent GSN station TAU located in Hobart, southern Tasmania, agrees well with past SWS studies of Vinnik et al. (1989) and Clitheroe and van der Hilst (1998). The results show that the fast shear wave polarization direction is approximately

ENE-WSW and parallel to the trend of the dominant surface structures in the area. These structures are likely related to a later phase of the Cambrian Tyennan Orogeny (Corbett et al., 1972), which represents the first phase of orogeny along the East Gondwana margin as a result of westward subduction of the Palaeo-Pacific plate. Another station “MOO” adjacent to TAU exhibits similar splitting parameters and together this may indicate that the lithosphere is the principal cause of the observed anisotropy in this region.

Moving northward into Bass Strait and south central Victoria (Selwyn Block), the systematic variation of strength and orientation of anisotropy across the stations (BA10, BA11, BA17, BA19, BA20, BA21, TOO) provides insight into how complex the tectonics of this region may have been. Few reliable splitting measurements were observed on King and Deal Islands owing to the low quality of the signal. Other possible contributing factors include the presence of complex upper mantle structures beneath the stations, including compositionally heterogeneous Selwyn Block (Cayley et al., 2002), and magma-induced heating of the upper mantle associated with the recent Quaternary Newer Volcanics Province. However, despite the fact that recent deformational events associated with breakup between Australia and Antarctica have possibly reworked previous anisotropy imprints, it is generally observed that splitting measurements in northwestern Tasmania through King Island to the southern tip of Victoria have a roughly similar fast polarisation direction of NE-SW. This trend is strongly correlated with magnetic signatures that can be traced from northwestern Tasmania to southern Victoria and are thought to be inherited from the Selwyn Block (Cayley et al., 2002). This suggests a tectonic affinity of the Selwyn block and northwest Tasmania and appears to support the presence of the so-called exotic Precambrian microcontinent VanDieland (Cayley, 2011; Moresi et al., 2014; Pilia et al., 2015b). We speculate that the microcontinent behaved as a rigid block, where the separation between Australia and Antarctica was forced to propagate along the Sorrel Fault System, preventing pervasive deformation of the microcontinent and retaining a substantially intact pattern of anisotropy since the Mesoproterozoic (Cayley, 2011). However, we note that our ability to retrieve a reliable anisotropy signature may be reduced by the lower signal to noise ratio of the Bass Strait islands dataset.

Stations BA05, BA06, BA07, BA08, BA09 and BA17 collectively indicate a rotation in fast

549 shear wave polarisation directions from NW-SE in the ETT (BA05, BA06) to NE in the
550 Furneaux Islands (BA07, BA08). This discrepancy between the ETT and the Furneaux
551 Islands may be due to the relatively recent breakup of Australia and Antarctica, which
552 resulted in lithospheric thinning, and subsequent formation of the three intracratonic rift
553 basins in Bass Strait that host the Furneaux Islands (Gunn et al., 1997; Gaina et al., 1998;
554 Fishwick and Rawlinson, 2012). Smaller delay times at the Furneaux Island stations
555 (~0.82±0.07 s (BA08) and ~0.68±0.06 s (BA09)) appear to suggest a positive correlation
556 with lithospheric thickness in this region (Kennett and Blewett, 2012; Fishwick et al., 2008).
557 In spite of this apparent correlation, there appears to be no correlation between the fast
558 polarisation direction and the absolute plate motion. Hence, anisotropy beneath ETT and the
559 Furneaux Islands appears to be primarily caused by fossil deformation recorded in the
560 lithosphere.
561
562 Our results demonstrate that the average delay times observed in southern Victoria are
563 considerably higher than in other parts of the study area. Measurements in the vicinity of the
564 Newer Volcanics Province (NVP) in southern Victoria show unusually large delay times for
565 which a primary contribution from the asthenospheric mantle is likely (e.g. Long et al.,
566 2009). Two possible scenarios that would result in unusually high delay times are: (1)
567 having an unusually thick anisotropic layer beneath the NVP. Because shear wave splitting
568 is inferred to be due to Lattice Preferred Orientation (LPO) of olivine in the asthenospheric
569 mantle, it is plausible that the thin lithosphere beneath the NVP is associated with a
570 correspondingly thick asthenosphere; (2) differences in upper mantle temperatures make
571 olivine LPO particularly strong in the anisotropic layer beneath the NVP (Karato et al.,
572 2007). Because of the large observed delay times, a model in which all of the anisotropy is
573 in the crust and mantle lithosphere would imply an unreasonably large magnitude of
574 anisotropy (roughly 20% anisotropy for a ~60 km thick lithosphere) and we can confidently
575 infer that the large delay times reflect contemporary flow in the asthenospheric mantle
576 (Rawlinson et al., 2017). While a small contribution to the observed splitting from crustal
577 anisotropy is likely, average values predicted from rock physics for crustal splitting are on
578 the order of perhaps ~0.1–0.3 s (Herquel et al., 1994; Savage, 1999). Maximum delay times
579 of 0.1 to 0.2 s per 10 km of homogeneously deformed crust might be expected (Barruol and
580 Mainprice, 1993). This could generate crustal delay times of up to ~0.8 s in southeast

Australia. Thus the large delay times observed here cannot be attributed primarily to crustal anisotropy. Even if we attribute 1 s of delay time to anisotropy in the crust and mantle lithosphere, the asthenosphere would have to contribute 1.5–2s of splitting beneath the NVP, which corresponds to ~6–8% anisotropy for a 150-km thick asthenosphere. Although these values are quite large compared to 3%, a value considered reasonable for a normal upper mantle, they are not out of the question. For example, Ben Ismaïl and Mainprice (1998) reported shear wave anisotropies larger that 11% and up to 15% in the upper mantle. However, these values were calculated for pure olivine crystals and they should reduce somewhat when the effect of 25–30 % of pyroxenes in lherzolites is taken into account (e.g., Mainprice and Silver, 1993).

Although we have largely interpreted the shear wave splitting results in terms of anisotropy frozen in the lithosphere and asthenospheric flow due to plate motion, we also consider an intriguing alternative in which we investigate φ as a function of angle by looking at results from stations surrounding Bass Strait. The overall fast polarisation direction appears to radiate outwards from the centre of Bass Strait. This observation could potentially be consistent with divergent mantle flow for a plate overriding a mantle plume. According to the plume theory (Wilson, 1963; Morgan, 1971), since the fast directions of anisotropy are determined by the spreading direction of the mantle, the fast polarisation directions (φ) of anisotropy around a mantle plume would be oriented vertically within the central upwelling and radiate outwards from the plume head (Rümpker and Silver, 2000; Ito et al., 2014). For example, Walker et al. (2001) studied shear wave splitting around the Hawaii hotspot and observed a spatial pattern in fast polarisation directions that they explained in terms of a parabolic asthenospheric flow model, in which a plume impinges on a moving lithospheric plate. Walker et al. (2005) invoked similar models to explain a semicircular pattern of fast polarisation directions in the vicinity of the Eifel hotspot and to explain the spatial distribution of fast polarisation directions in the eastern Snake River Plain adjacent to the Yellowstone hotspot (Walker et al., 2004). With the superimposed influence of absolute plate motion, horizontal flow away from the central plume head upwelling is predicted to be parabolic (Walker et al., 2005). This is a model that combines the effect of mantle upwelling with APM, resulting in parabolic flow in the asthenosphere, and has been successful at explaining patterns of fast polarisation directions in some regions associated with mantle upwelling, but has proved less successful in regions such as Afar (Gashawbeza et al., 2004;

Walker et al., 2005) or Iceland (Walker et al., 2005).

Previous studies by Davies et al. (2015) identify the world's longest continental hotspot track (over 2000 km long) which begins in north Queensland, and extends southward, possibly as far as NW Tasmania. The plume source of the hotspot track may be responsible for the observed pattern of fast polarisation directions surrounding Bass Strait. However, further evidence would be required if such a theory was to gain traction; apart from plate motion model predictions of the current plume source, there is very little evidence to suggest that it still exists, apart from reduced uppermost mantle velocities imaged by regional surface wave tomography (Fishwick and Rawlinson, 2012). Recent studies indicate that the plume waned during its traverse of the Australian continent, and it may now have dissipated completely (Rawlinson et al., 2017).

Overall, the complicated SKS waveforms and splitting patterns observed in the study area are plausibly due to multiple layers of anisotropy, asthenospheric contribution to the anisotropy, considerable lateral heterogeneity, complex lithospheric keels (i.e., Vinnik et al., 1989, 1992; Barruol and Hoffmann, 1999; Heintz and Kennett, 2005), or a combination of these factors. Without detailed modelling, which the backazimuthal coverage will not permit, it is difficult to untangle the relative contributions to the observed splitting from the lithospheric vs. asthenospheric upper mantle, but we can say with confidence that the lithosphere and/or crust likely makes a significant contribution to the splitting signal in this region.

6.2 Comparison with magnetic anomalies

Despite the limited number of reliable measurements obtained at some stations largely due to high noise levels, particularly in the island stations in Bass Strait and northern Tasmania, direct correlations can still be observed between the measured orientation of the polarization plane of the fast shear-waves and the mapped near-surface structures from the magnetic data (Fig. 11). The NE-SW linear structures of alternating positive and negative magnetic anomalies in northwest Tasmania are presumed to represent magmatic dikes of the Mount Reid Volcanics (Crawford et al., 2003; Berry, 1995; Seymour et al., 2007). There is a good correlation between fast shear wave splitting directions (φ) and magnetic lineaments in NW

Tasmania. However, ETT and Furneaux Islands are devoid of any correlation between fast shear wave splitting directions (φ) and magnetic lineaments, which are considerably weaker compared to those observed in eastern Bass Strait. In the Lachlan Orogen, the magnetic anomalies and fast shear wave splitting directions (φ) are parallel to the structural trend of the Lachlan Fold Belt. However, the correlation in southern Victoria and the Bass Strait islands is poor.

Magnetic anomalies reflect a contrast in upper crustal composition and/structural fabric (Kletetschka and Stout, 1998). An alignment between fast splitting directions (associated with the upper mantle) and crustal magnetic lineaments thus implies the presence of vertically coherent deformation (VCD). This helps support the idea that anisotropy frozen in the lithosphere is the main source of anisotropy in this region.

6.3 Comparison with crustal anisotropy measurements from surface wave tomography

One of the well-known limitations of shear-wave splitting analysis is its inability to resolve the depth distribution of anisotropy. By contrast radial variations in anisotropy can be assessed by surface wave data, which samples different depth ranges as a function of period. However, surface wave anisotropy measurements have significantly poorer lateral resolution than shear wave splitting measurements. Despite the fact that these two measurements do not identically sample the lithosphere, we believe that a comparison of our splitting measurements with the crustal anisotropy measurements of Pilia et al. (2016) will shed more light on the characteristics of the anisotropy in our study area (Fig. 12). Upon comparing the weighted mean of SKS/SKKS splits with the 5 second period Rayleigh wave phase anisotropy variations in the crust, it can be seen that the fast polarisation direction (φ) along the Lachlan Fold Belt and southern Victoria are quite consistent; this supports our earlier contention that lithospheric anisotropy is envisaged to be the dominant contributor in this region. In Bass Strait the φ measurements seem to be quite consistent in both models. It is interesting to note that measurements in Tasmania have 90° inconsistencies in φ. Even though this anomaly did not manifest when comparing our results with magnetic structures, crust-mantle decoupling cannot be completely ruled out. Another, perhaps more likely,

interpretation is that the surface wave anisotropy is restricted to the upper crust, and therefore does not dominate the shear wave splitting signal.

7. Conclusions

New results from the shear wave splitting data set presented in this study provide a first-order picture of anisotropy and deformation in the upper mantle beneath Bass Strait and the adjoining land masses and yields constraints on the different tectonic terranes in southeast Australia. Despite uneven station distribution, noisy data recorded on the islands in the study area, and a complex tectonic history, we were able to highlight coherent patterns of anisotropy from shear wave splitting in different parts of the study area.

Evidence of fast shear wave splits being polarised in directions oriented parallel to the local structural trends (e.g. northwest Tasmania and Selwyn Block and along the Lachlan Fold Belt) may account for deformation induced LPO anisotropy frozen in the lithosphere. The strong anisotropy observed beneath NVP possibly reflects an anisotropy contribution from thick asthenosphere underlying a thin lithosphere. The overall fast polarisation that appears to radiate outwards from the centre of Bass Strait could alternatively be the result of plume-induced anisotropy, although we acknowledge that evidence for a plume in this region is limited. However, based on evidence from various sources including crustal surface wave tomography, it is difficult to interpret the occurrence of complex patterns of anisotropy and abnormally large delay times from shear wave splitting beneath southeast Australia in terms of either mantle-flow related anisotropy or anisotropy frozen in the lithosphere: a contribution from both the lithospheric and sublithospheric mantle is likely. The poor backazimuthal coverage is not sufficient to be able to pin down the contribution from each source of anisotropy by, for instance, performing two-layer modelling of the anisotropy.

In an attempt to understand the depth-distribution of anisotropy we compared the observed fast polarisation directions with other datasets: (1) the fast polarisation directions vary for each tectonic unit, indicating a dominant lithospheric “fossil” anisotropy. This interpretation is supported by (2) poor correlation of fast polarisation direction with plate motion direction, which may be parallel only by chance at a few stations and thus does not reflect large scale

asthenospheric process; (3) the trend of magnetic structures aligns well with the observed fast polarisation directions at many of the analysed stations. This suggests vertically coherent deformation throughout the crust and upper-most mantle and supports the idea that splitting measurements reflect the most recent tectonic event; (4) there is also a consistency between (crustal) azimuthal anisotropy directions and our teleseismic shear wave splitting fast polarisation directions in mainland Australia and Bass Strait, but the anisotropy directions of the two different measurements appear to be roughly orthogonal in Tasmania. Even though this anomaly did not manifest in the comparison of our results with magnetic structures, crust-mantle decoupling cannot be completely ruled out. Alternatively, the pattern of surface wave anisotropy observed may simply be an upper crustal feature, and hence only makes a small contribution to the shear wave splitting signal which is otherwise dominated by the lower crust and upper mantle.

Acknowledgements

The work contained in this paper was conducted during a PhD study funded by Abubakar Tafawa Balewa University, Bauchi, Nigeria and University of Aberdeen, UK. We thank field teams working through UTAS and ANU, and Armando Arcidiaco and Qi Li, ANU, for assistance with collection and archiving of the BASS data used in this study. Australian Research Council grant LP110100256 was instrumental in supporting the BASS deployment. We also thank Geoscience Australia and IRIS for providing part of the data used in this study.

References

Argus, D. F., Gordon, R. G. & DeMets, C. (2011). Geologically current motion of 56 plates relative to the no-net-rotation reference frame. Gechemistry, Geophysics, Geosystems 12, Q11001, DOI:10.1029/2011GC003751.

Barbuska, V. & Cara, M. (1991). Seismic anisotropy in the Earth. Kluwer Academic Publishers, 1991, 217 pp.

Barruol, G. & Hoffman R. (1999). Seismic anisotropy beneath the Geoscope stations from SKS splitting. Journal of Geophysical Research 104, 10757–10774.

Bastow, I., Owens, T., Helffrich, G. & Knapp, J. (2007). Spatial and temporal constraints on sources of seismic anisotropy: Evidence from the Scottish highlands. Geophys. Res. Lett. 34, L05305, DOI:10.1029/2006GL028911.

Becker, T. W., Browaeys, J. T. & Jordan, T. H. (2007). Stochaastic analysis of shear-wave splitting length scales. Earth and Planetary Sci. Letters 259, 526-540.

Berry, R. F. (1995). Tectonics of western Tasmania: Late Precambrian–Devonian, in: COOKE, D. R.; KITTO, P. A. (ed.). Contentious issues in Tasmanian geology. Abstracts Geological Society of Australia 39, 6–8.

Berry, R. F., Chmielowski, R. M., Steele, D. A. & Maffre, S. (2007). Chemical U – Th – Pb monazite dating of the Cambrian Tyennan Orogeny, Tasmania. Australian Journal of Earth Sciences 54:5, 757-771, DOI: 10.1080/08120090701305269.

Ben Ismaïl, W. & Mainprice, D. (1998). A statistical view of the strength of seismic anisotropy in the upper mantle based on petrofabric studies of ophiolite and xenolith samples. Tectonophysics 296, 145–157.

Betts, P.G., Giles, D. Lister, G.S. & Frick, L.R. (2002). Evolution of the Australian lithosphere. Aust. J. Earth Sci. 49, 661 – 695.

Berry, R. F. & Crawford, A. J. (1988). The tectonic significance of Cambrian allochthonous mafic-ultramafic complexes in Tasmania. Australian Journal of Earth Sciences 35, 523–533.

Black, L. P., McClenagan, M. P., Korsch, R. J., Everard, J. L., Calver, C. R., Seymour, D. B., Reed, A. & Foudoulis, C. (2004). Using SHRIMP to decipher the history of middle Paleozoic magmatism in Tasmania. Geological Society of Australia Abstracts v. 73, 55.

Blackman, D. & Kendall, J. -M. (1997). Sensitivity of teleseismic body waves to mineral texture and melt in the mantle beneath a mid-ocean ridge. Philos. Trans. R. Soc. A, 355, 217–231, DOI:10.1098/rsta.1997.0007.

767 Burton, G. R., & Triggs, S. J. (2014). Discussion of Glen R. A., Korsch R. J., Hegarty R., Saeed A., Poudjom
768 Djomani Y., Costelloe R. D. & Belousova E. (2013). Geodynamic significance of the boundary between the
769 Thomson Orogen and the Lachlan Orogen, northwestern New South Wales and implications for Tasmanide
770 tectonics. Australian Journal of Earth Sciences 60, 371–412. Australian Journal of Earth Sciences 61:4, 639-
771 641, http://dx.doi.org/10.1080/08120099.2014.903857

772 Cayley, R. (2011). Exotic crustal block accretion to the eastern Gondwanaland margin in the Late Cambrian–
773 Tasmania, the Selwyn Block, and implications for the Cambrian–Silurian evolution of the Ross, Delamerian,
774 and Lachlan orogens. Gondwana Research, 19, 628–649. http://dx.doi.org/10.1016/j.gr.2010.11.013.

775 Cayley R., Taylor, D. H., VandenBerg, A. H. M. & Moore, D. H. (2002). Proterozoic Early Palaeozoic rocks
776 and the Tyennan Orogeny in central Victoria: the Selwyn Block and its tectonic implications. Australian
777 Journal of Earth Sciences 49, 225 – 254.

778 Clitheroe, G. & van der Hilst, R. (1998). Complex anisotropy in the Australian lithosphere from shear wave
779 splitting in broadband records. AGU Geophysical Monographs.

780 Corbett, K. D., Banks, M. R. & Jago, J. B. (1972). Plate tectonics and the Lower Palaeozoic of Tasmania,
781 Nature Phys. Sci. 240, 9 – 11.

782 Crampin, S. (1994). The Fracture criticality of crustal rocks. Geophys. J. Int. 118, 428-438.

783 Crawford, A. J. & Berry, R. F. (1992). Tectonic implications of Late Proterozoic–Early Palaeozoic igneous
784 rock associations in western Tasmania. Tectonophysics 214, 37–56.

785 Crawford, A., Meffre, S. & Symonds, P. (2003). 120 to 0 Ma tectonic evolution of the southwest Pacific and
786 analogous geological evolution of the 600 to 220 Ma Tasman Fold Belt System. Special Papers—Geological
787 Society of America, 383–404.

788 Davies, D.R., Rawlinson, N., Iaffaldano, N. & Campbell, I.H. (2015). Lithospheric controls on magma
789 composition along Earth's longest continental hotspot track. Nature 525, 511–514.

790 Debayle, E. & Kennett, B.L.N. (1998). Anisotropy in the Australian upper mantle from waveform inversion,
791 Ann. Geophys. 16, 37.

792 Debayle, E. & Kennett, B.L.N. (2000). The Australian continental upper mantle: Structure and deformation
793 inferred from surface waves, J. Geophys. Res. 105, 25423-25450. DOI:10.1029/2000JB900212.

794 Debayle, E. (1999). SV-wave azimuthal anisotropy in the Australian upper mantle: preliminary results from
795 automated Rayleigh waveform inversion, Geophys. J. Int. 137, 747 – 754.

796 Direen, N.G. & Crawford, A.J. (2003). The Tasman Line: where is it, what is it, and is it Australia's Rodinian
797 breakup boundary? Australian Journal of Earth Sciences 50, 491–502. http://dx.doi.org/10.1046/j.1440-
798 0952.2003.01005.x.

799 Eaton, D., Frederiksen, A. & Miong, S.-K. (2004). Shear-wave splitting observations in the lower Great
800 Lakes region: Evidence for regional anisotropic domains and keel-modified asthenospheric flow, Geophys.
801 Res. Lett. 31, L07610, DOI:10.1029/2004GL019438.

802 Elliot, C. G., Woodward, N., B. & Gray, D. R. (1993). Complex regional fault history of the Badger Head
803 region, northern Tasmania. Aust. J. Earth Sci. 40, 155 – 168.

804 Fergusson, C. L. (2009). Tectonic evolution of the Macquarie Arc, central New South Wales. Arguments for
805 subduction polarity & anticlockwise rotation. Australian Journal of Earth Sciences 56, 179 - 193.

806 Fergusson, C. L. (2014). Discussion on 'Refining accretionary orogen models for the Tasmanides of eastern
807 Australia' by R. A. Glen. Australian Journal of Earth Sciences 61. DOI:10.1080/ 08120099.2014.917334.

808 Fishwick, S., Heintz, M., Kennett, B. L. N., Reading, A. M. & Yoshizawa, K. (2008). Steps in lithospheric
809 thickness within eastern Australia, evidence from surface wave tomography. Tectonics v. 27, TC0049, DOI:
810 10.129/2007TC002116.

811 Fishwick, S. & Rawlinson, N. (2012). 3-D structure of the Australian lithosphere from evolving seismic
812 datasets. Australian Journal of Earth Sciences 59, 809-826.
813
814 Foster, D. A. & Gray, D. R. (2000). Evolution and structure of the Lachlan Fold Belt (Orogen) of eastern
815 Australia. Annual Reviews of Earth and Planetary Sciences 28, 47 – 80.

816 Fouch, M. J., Fischer, K. M., Parmentier, E., Wysession, M. E. & Clarke, T. J. (2000). Shear wave splitting,
817 continental keels, and patterns of mantle flow. J. Geophys. Res. 105(B3), 6255–6275,
818 DOI:10.1029/1999JB900372.

819 Frederiksen, A., Miong, S.-K., Darbyshire, F., Eaton, D., Rondenay, S. & Sol, S. (2007). Lithospheric
820 variations across the Superior Province, Ontario, Canada: Evidence from tomography and shear wave
821 splitting. J. Geophys. Res. 112, B07318, DOI:10.1029/2006JB004861.

822 Gaina, C., Muller, D., Royer, J. -Y., Stock, J., Hardebeck, J. & Symonds, P. (1998). The tectonic history of
823 the Tasman Sea: a puzzle with 13 pieces. J. Geophys. Res. 103, 12,413-12,433.

824 Gashawbeza, E. M., Klemperer, S. L., Nyblade, A. A., Walker, K. T. & Keranen, K. M. (2004). Shear-wave
825 splitting in Ethiopia: Precambrian mantle anisotropy locally modified by Neogene rifting, Geophys. Res.
826 Lett. 31, L18602. http://dx.doi.org/ 10.1029/2009JB007141.

827 Graeber, F. M., Houseman, G. A. & Greenhalgh, S. A. (2002). Regional teleseismic tomography of the
828 western Lachlan Orogen and the Newer Volcanic Province, southeast Australia. Geophy. J. Int. 149, 249–
829 266.

830 Girardin, N. & Farra, V. (1998). Azimuthal anisotropy in the upper mantle from observations of P-to-S
831 converted phases: Application to southeast Australia. Geophys. J. Int. 133, 615-629.

832 Glen, R. A. (2005). The Tasmanides of eastern Australia. In A. P. M. Vaughan, P. T. Leat, & R. J. Pankhurst
833 (Eds.), Terrane processes at the margins of Gondwana (Vol. 246. pp. 23-96). London: Geological Society,
834 London, Special Publication.

835 Glen, R.A. (2013). Refining accretionary orogen models for the Tasmanides of eastern Australia. Aust. J.
836 Earth Sci. 60, 315–370.

837 Glen, R. A., Poudjom Djomani, Y. H., Belousova, E., Hegarty, R. & Korsch, R. J. (2014). Geodynamic
838 significance of the boundary between the Thomson Orogen and the Lachlan Orogen, northwestern New
839 South Wales and implications for Tasmanide tectonics: Reply. Australian Journal of Earth Sciences 61, 643-
840 657.

841 Gray, D. R. & Foster, D. A. (2004). Tectonic evolution of the Lachlan Orogen, southeastern Australia:
842 historical review, data synthesis and modern perspectives. Australian Journal of Earth Sciences 51, 773-817.

843 Gripp, A.E. & Gordon, R.G. (2002). Young tracks of hotspots and current plate velocities. Geophys. J. Int.
844 150, 321 – 361.

Heintz, M. & Kennett, B. L. N. (2005). Continental scale shear wave splitting analysis: Investigation of seismic anisotropy underneath the Australian continent. Earth and Planetary Science Letters 236, 106–119.

Herquel, G., Wittlinger, G. & Guilbert, J. (1995). Anisotropy and crustal thickness of Northern-Tibet. New constraints for tectonic modelling, Geophys. Res. Lett. 22, 1925-1928.

Holm, O. H., Berry, R. F. (2002). Structural history of the Arthur Lineament, northwest Tasmania: an analysis of critical outcrops. Australian Journal of Earth Sciences 49, 167–185.

Ito, G., Dunn, R., Li, A., Wolfe, C. J., Gallego, A. & Fu, Y. (2014). Seismic anisotropy and shear wave splitting associated with mantle plume-plate interaction, J. Geophys. Res. Solid Earth 119, DOI:10.1002/2013JB010735.

Karato, S., Jung, H., Katayama, I. & Skemer, P. (2008). Geodynamic significance of seismic anisotropy of the upper mantle: new insights from laboratory studies, Annual Rev. Earth Planet. Sci. 36, 59-95.

Kennett, B. L. N., & Blewett, R. S. (2012). Lithospheric framework of Australia, Episodes Vol. 35(1), 9-22.

Kletetschka, G. & Stout, J. H. (1998). The origin of magnetic anomalies in lower crustal rocks, Labrador. Geophys. Res. Letters Vol. 25, No. 2, 199-202.

Leaman, D., Baillie, P. & Powell, C.M. (1994). Precambrian Tasmania: a thin-skinned devil. Exploration Geophysics 25, 19–23. DOI:10.1071/EG994019.

Levin, V., Menke, W. & Park, J. (1999). Shear wave splitting in the Appalachians and the Urals: A case for multilayered anisotropy. J. Geophys. Res. 104, 17, 975–17,993, DOI:10.1029/1999JB900168.

Lister, G.S., Ethridge, M.A. & Symonds, P.A. (1991). Detachment models for the formation of passive continental margins. Tectonics 10, 1038–1064.

Long, M. D., Gao, H., Klaus, A., Wagner, L. S., Fouch, M. J., James, D. E. & Humphreys, E. (2009). Shear wave splitting and the pattern of mantle flow beneath eastern Oregon. Earth and Planetary Science Letters 288, 359–369.

Long, M. D. & Silver, P.G. (2009). Shear wave splitting and Mantle anisotropy: Interpretations, and new directions. Surveys in Geophysics 30, 407–461.

875 Long, M. D. & Becker, T. W. (2010). Mantle dynamics and seismic anisotropy. Earth and Planetary Science
876 Letters 297, 341–354.

877 Mainprice, D., Barruol, G. & Ben Ismaïl, W. (2000). The seismic anisotropy of the Earth's mantle: from
878 single crystal to polycrystal. In: S.I. Karato, A. Forte, R.C. Liebermann, G. Masters and L. Stixrude
879 (Editors), Earth's deep interior: Mineral Physics and Tomography from the atomic to the global scale.
880 Geophysical Monograph. AGU, Washington, D.C., 237-264.
881
882 Mainprice, D. & Silver, P.G. (1993). Interpretation of SKS waves using samples from the subcontinental
883 lithosphere. Phys. Earth Planet. Inter. 78, 257–280.

884 Meffre, S., Berry, R. F. & Hall, M. (2000). Cambrian metamorphic complexes in Tasmania: tectonic
885 implications. Australian Journal of Earth Sciences 47, 971–985.

886 Milligan, P. R., Franklin, R., Minty, B. R. S., Richardson, L. M. & Percival, P. J. (2010). Magnetic anomaly
887 map of Australia (Fifth edition), 1:15 000 000 scale, Geoscience Australia, Canberra.

888 Moore, D. H., Betts, P. G. & Hall, M. (2013). Towards understanding the early Gondwana margin in
889 southeastern Australia. Gondwana Research 23, 1581-1598.

890 Moore, D. H., Betts, P. G. & Hall, M. (2015). Fragmented Tasmania: the transition from Rodinia to
891 Gondwana. Australian Journal of Earth Sciences 62, 1-35.

892 Moresi, L., Betts, P. G., Miller, M. S. & Cayley, R. A. (2014). Dynamics of continental accretion. Nature
893 508, 245 - 248.

894 Morgan, W. J. (1971). Convection plumes in the lower mantle. Nature 230, 42 - 43.

895 Nicolas, A. & Christensen N. I. (1987). Formation of anisotropy in upper mantle peridotite. Geodyn. Ser. 16,
896 111-123.

897 Ozalaybey, S. & Chen, W.-P. (1999). Frequency-dependent analysis of SKS/SKKS waveforms observed in
898 Australia: evidence for null birefringence, Phys. Earth Planet. Inter. 114, 197 – 210.

899 Pilia, S., Rawlinson, N., Green, N., Reading, A. M., Cayley, R., Pryer, L., Arroucau, P. & Duffet, M. (2015a).

Linking mainland Australia and Tasmania using ambient seismic noise tomography: Implications for the tectonic evolution of the east Gondawana margin. Gondwana Research 28, 1212-1227.

Pilia, S., Rawlinson, N., Cayley, R.A., Musgrave, R., Reading, A.M., Direen, N.G. & Young, M.K. (2015b). Evidence of micro-continent entrainment during crustal accretion. Sci. Rep., 5. http://dx.doi.org/10.1038/srep/08218.

Pilia, S., Arroucau, P., Rawlinson, N., Reading, A.M. & Cayley, R.A. (2016). Inherited crustal deformation along the East Gondwana margin revealed by seismic anisotropy tomography. Geophysical Research Letters 43 (23), 12,082-12,090. ISSN 0094–8276, DOI: 10.1002/2016GL071201.

Rawlinson, N., Reading, A.M. & Kennett, B.L.N. (2006). Lithospheric structure of Tasmania from a novel form of teleseismic tomography. Journal of Geophysical Research 111, http://dx.doi.org/10.1029/2005JB003803.

Rawlinson N. & Urvoy M. (2006). Simultaneous inversion of active and passive source datasets for 3-D seismic structure with application to Tasmania. Geophysical Research Letters 33, DOI:10.1029/2006GL028105.

Rawlinson, N. & Kennett, B. L. N. (2008). Teleseismic tomography of the upper mantle beneath the southern Lachlan Orogen. Physics of the Earth and Planetary Interiors 167, 84–97.

Rawlinson, N. & Fishwick, S. (2011). Seismic structure of the southeast Australian lithosphere from surface and body wave tomography. Tectonophysics, DOI:10.1016/j.tecto.2011.11.016.

Rawlinson, N., Kennett, B. L. N., Salmon, M. & Glen, R. A. (2015). Origin of lateral heterogeneities in the upper mantle beneath Southeast Australia from seismic tomography. In: Khan, A., Deschamps, F. (Eds.), The Earth's Heterogeneous Mantle: A Geophysical, Geodynamical and Geochemical Perspective, Springer Geophysics. Springer, 47–78.

Rawlinson, N., Pilia, S., Young, M. Salmon, M. & Yang, Y. (2016). Crust and upper mantle structure beneath southeast Australia from ambient noise and teleseismic tomography. Tectonophysics 689, 143-156. http://dx.doi.org/10.1016/j.tecto.2015.11.034.

Rawlinson, N., Davies, D. R. & Pilia S. (2017). The mechanisms underpinning Cenozoic intraplate volcanism in eastern Australia: Insights from seismic tomography and geodynamic modeling. Geophys. Res. Lett. 44, 9681–9690, DOI:10.1002/2017GL074911.

Reed, A. R., Calver, C. & Bottrill, R.S. (2002). Palaeozoic suturing of eastern and western Tasmania in the west Tamar region: implications for the tectonic evolution of southeast Australia. Australian Journal of Earth Sciences 49, 809–830.

Reed, A. R. (2001). Pre-Tabberabberan deformation in eastern Tasmania: a southern extension of the Benambran Orogeny. Australian Journal of Earth Sciences 48, 785–796. http://dx.doi.org/10.1046/j.1440-0952.2001.00900.x.

Rosenbaum, G., Pengfei, L. & Rubatto, D. (2012). The contorted New England Orogen (eastern Australia): new evidence from U–Pb geochronology of early Permian granitoids. Tectonics 31. http://dx.doi.org/10.1029/2011TC002960.

Rümpker, G. & Silver, P.G. (2000). Calculating splitting parameters for plume-type anisotropic structures of the upper mantle, Geophys. J. Int. 143, 507–520.

Savage, M. (1999). Seismic anisotropy and mantle deformation: What have we learned from shear wave splitting, Rev. Geophys. 37, 65–106, DOI:10.1029/98RG02075.

Seymour, D. B., Green, G. R. & Calver, C. R. (2007). The Geology and Mineral Deposits of Tasmania: a summary. Geological Survey Bulletin 72, Second Edition, ISBN 0 7246 4017 7.

Siégel, C., Bryan, S. E., Allen, C. M., Purdey, D. J., Cross, A. J., Uysal, I. T. & Gust, D. A. (2018). Crustal and thermal structure of the Thomson Orogen: constraints from the geochemistry, zircon U-Pb age, and Hf and O isotopes of subsurface granitic rocks. Australian Journal of Earth Sciences, DOI: 10.1080/08120099.2018.1447998.

Silver, P.G. & Chan, W.W. (1988). Implications for continental structure and evolution from seismic anisotropy, Nature 335, 34–39.

Silver, P.G. & Chan, W.W. (1991). Shear wave splitting and subcontinental mantle deformation. J. Geophys. Res. 96, 16,429–16,454.

Silver, P.G. & Savage, M.K. (1994). The interpretation of shear-wave splitting parameters in the presence of two anisotropic layers. Geophys. J. Int. 119, 494–963.

954 Silver, P.G. (1996). Seismic anisotropy beneath the continents: probing the depths of geology. Annu. Rev.
955 Earth Planet. Sci. 24, 385–432.

956 Simons, F.J. & Van der Hilst, R.D. (2003). Seismic and mechanical anisotropy and the past and present
957 deformation of the Australian lithosphere. Earth Planet. Sci. Lett. 211, 271 – 286.

958 Sleep, N., Ebinger, C. & Kendall, J. -M. (2002). Deflection of mantle plume material by cratonic keels. Geol.
959 Soc. London Spec. Publ. 199, 135–150, DOI:10.1144/GSL.SP.2002.199.01.08.

960 Spampinato, G. P. T., Ailleres, L., Betts, P. G. & Armit, R. J. (2015). Crustal architecture of the Thomson
961 Orogen in Queensland inferred from potential field forward modelling. Australian Journal of Earth Sciences
962 62:5, 581-603, DOI: 10.1080/08120099.2015.1063546.

963 Stotz, I.L., Iaffaldano, G. & Davies, D.R. (2018). Pressure-Driven Poiseuille Flow: A Major Component of
964 the Torque-Balance Governing Pacific Plate Motion. Geophys. Res. Lett. 45(1), 117-125,
965 DOI:10.1002/2017GL075697.
966
967 Teanby, N., Kendall, J. -M. & Van der Baan, M. (2004). Automation of shear-wave splitting measurements
968 using cluster analysis. Bull. Seismol. Soc. Am. 94, 453–463, DOI:10.1785/0120030123.

969 Tommasi, A. (1998). Forward modeling of the development of seismic anisotropy in the upper mantle. Earth
970 Planet. Sci. Lett. 160, 1-13.

971 Turner, N., Black, L. P. & Kamperman, M. (1998). Dating of Neoproterozoic and Cambrian orogenesis in
972 Tasmania. Aust. J. Earth. Sci. 45, 789–806.

973 van der Beek, P. A., Braun, J. & Lambeck, K. (1999). Post-Paleozoic uplift history of southeastern Australia
974 revisited: Results from a process-based model of landscape evolution, Aust. J. Earth Sci. 46, 157-172.

975 Vauchez, A. & Nicolas, A. (1991). Mountain building: Strike-parallel motion and mantle anisotropy.
976 Tectonophysics 185, 183–201, DOI: 10.1016/0040-1951(91) 90443-V.

977 Vinnik, L. P., Kosarev, G. L. & Makeyeva, L. I. (1984). Anisotropiya litospery po nalblyudeniyam vol SKS
978 and SKKS, Dokl. Akad. Nauk USSR 278, 1335-1339.

979 Vinnik, L., Farra, V. & Romanowicz, B. (1989). Azimuthal anisotropy in the Earth from observations of SKS
980 at Geoscope and NARS broadband stations, Bull. Seismol. Soc. Am. 79, 1542–1558.

981 Vinnik, L., Makeyeva, L., Milev, A. & Usenko, A. Y. (1992). Global patterns of azimuthal anisotropy and
982 deformations in the continental mantle, Geophys. J. Int. 111, 433–447.

983 Walker, K. T., Nyblade, A.A., Klemperer, S.L., Bokelmann, G.H.R. & Owens, T.J. (2004). On the
984 relationship between extension and anisotropy: constraints from shear wave splitting across the East African
985 plateau, J. geophys. Res. 109**,** 1–21.

986 Walker, K. T., Bokelmann, G.H. R., Klemperer, S.L. & Bock, G. (2005). Shear-wave splitting around the
987 Eifel hotspot: evidence for a mantle up- welling, Geophys. J. Int. 163**,** 962–980.

988 Williams, E. (1989). Summary and synthesis, in Geology and Mineral Resources of Tasmania, edited by C. F.
989 Burrett and E. L. Martin, Spec. Publ. Geol. Soc. Aust. 15, 468 – 499.

990 Wilson, J. T. (1963). A possible origin of Hawaiian Islands, Can. J. Phys. 41, 863-870.

991 Zhang, S. & Karato, S. (1995). Lattice preferred orientation of olivine aggregates deformed in simple shear,
992 Nature 375, 774 – 777.

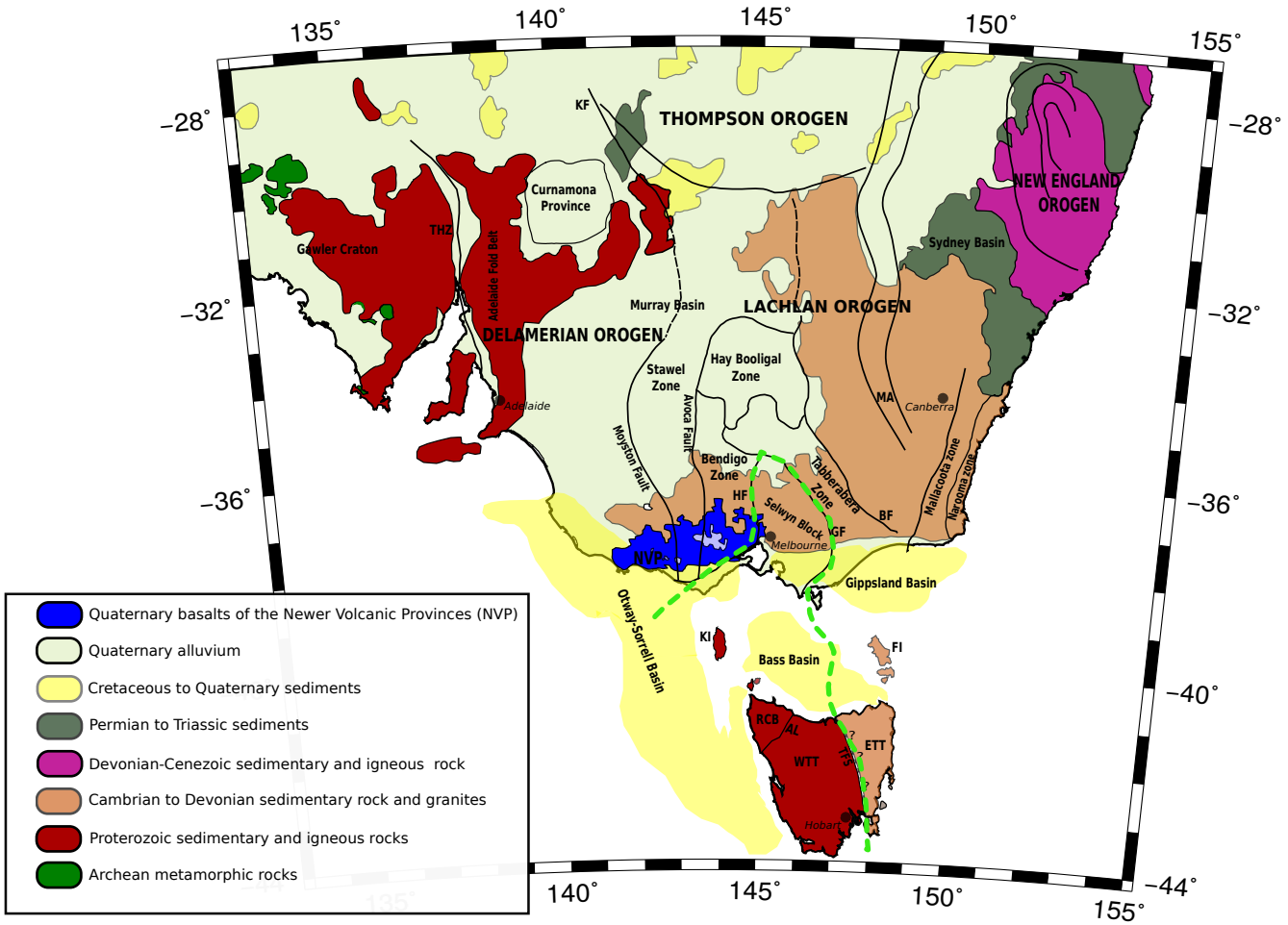

Fig. 1: Simplified geological map of southeastern Australia showing observed and inferred geological boundaries and main tectonic features mentioned in the text. Thick black lines show locations of structural boundaries. Thick green dashed line denotes the boundary of VanDieland. KF = Koonenberry Fault; HF = Heathcote Fault; GF = Governor Fault; BF = Bootheragandra Fault; THZ = Torrens Hinge Zone; NVP = Newer Volcanic Province; MA = Macquarie Arc; KI = King Island and FI = Flinders Island in Bass Strait; WTT = Western Tasmania Terrane; ETT = Eastern Tasmania Terrane; AL = Arthur Lineament; TFS = Tamar Fracture System and RCB = Rocky Cape Block.

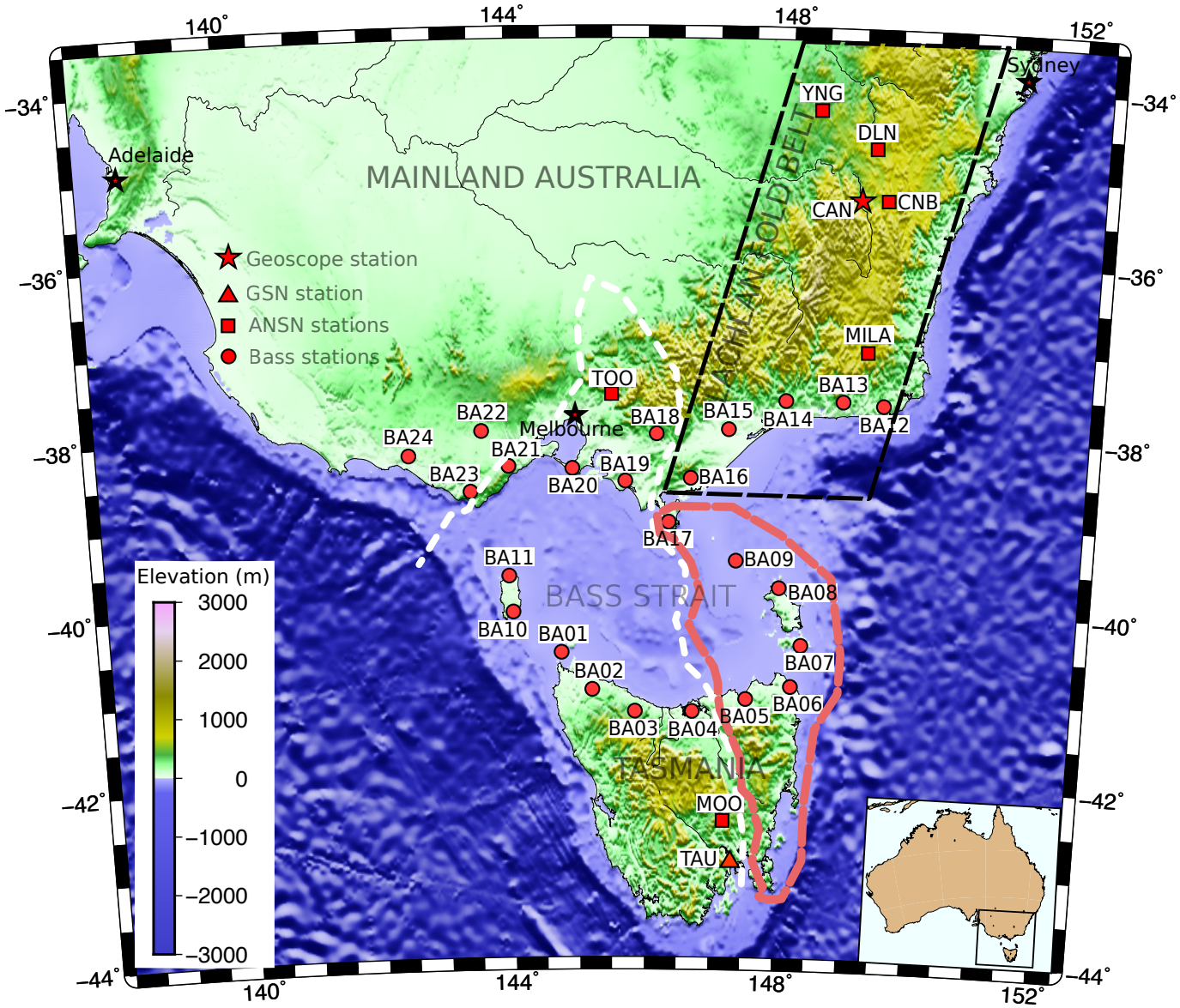

Fig. 2: Topographic/bathymetric map of the study area showing main tectonic blocks and locations of the 32 broadband instruments mentioned in the text. Thick white dashed line denotes the boundary of VanDieland. Thick red dashed line outlines the boundary of East Tasmania terranne and Furneaux Islands. Thick black dashed line highlights part of the Lachlan Fold Belt.

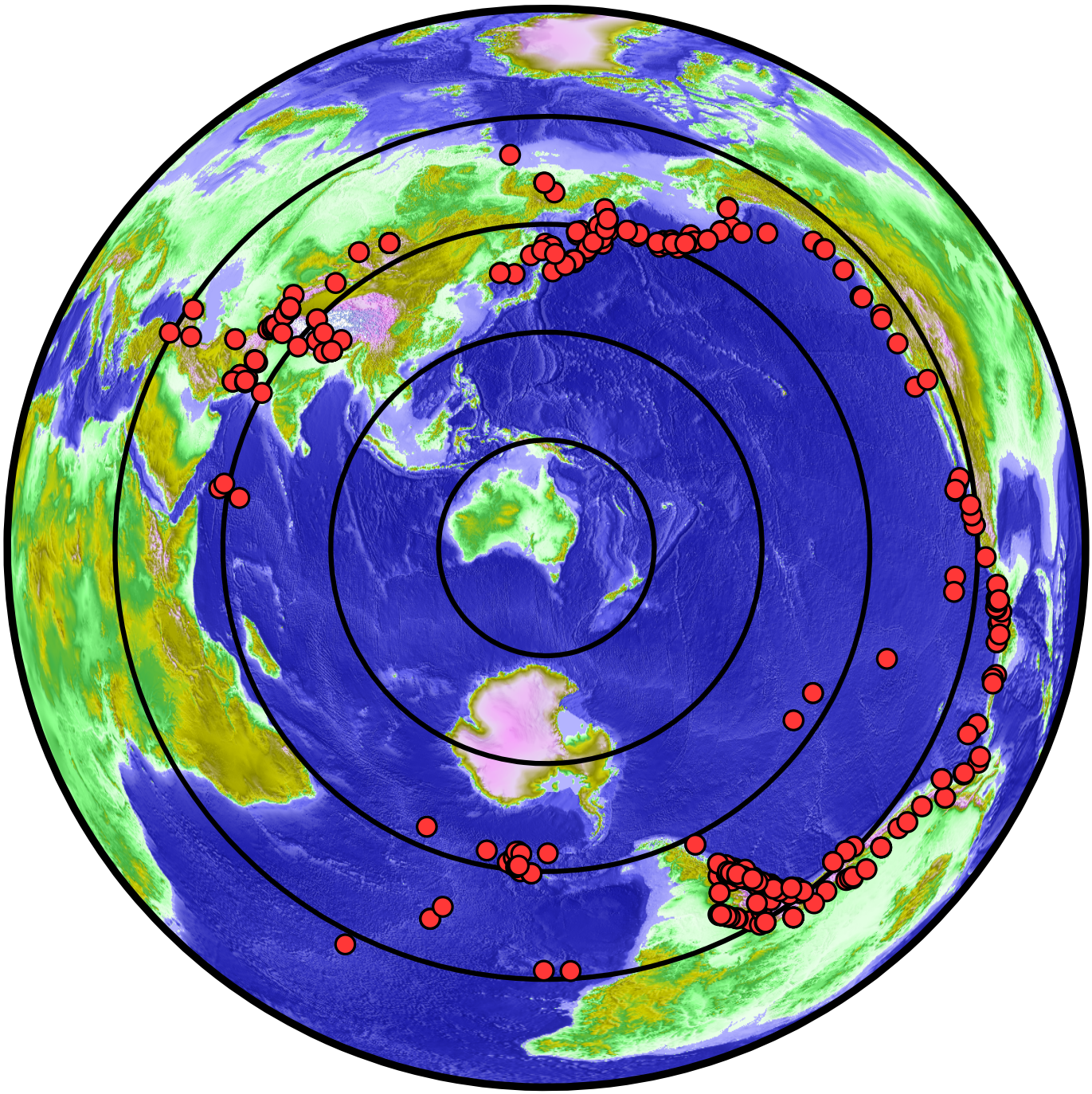

Fig. 3: Distribution of teleseismic events used for this study. Concentric circles are plotted at 30° intervals from the centre of Bass Strait.

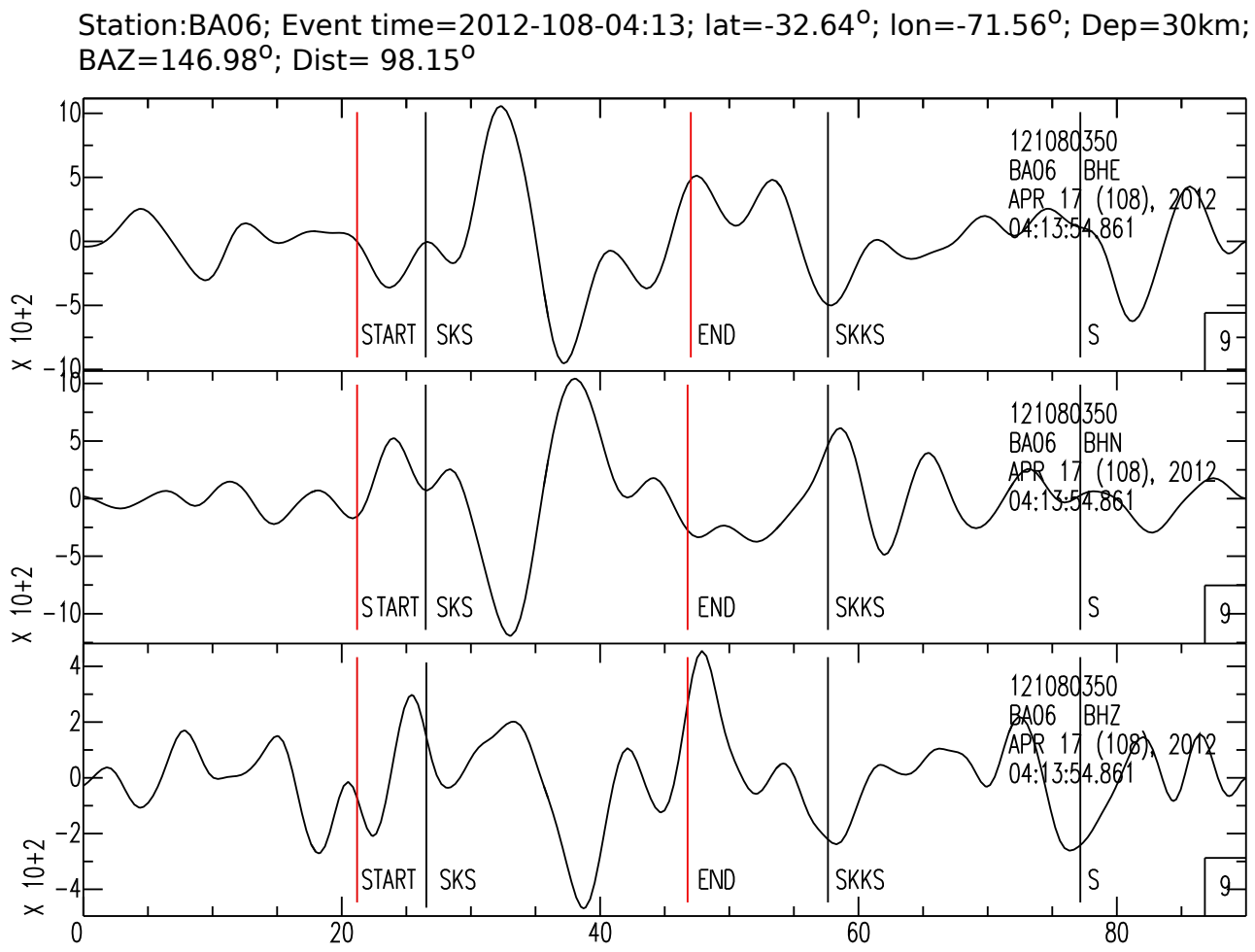

Fig. 4: Example of a filtered seismogram at station BA06, with the expected arrival times for SKS and SKKS from the ak135 earth model shown. Red vertical lines represent the time window chosen for analysis (marked START and END).

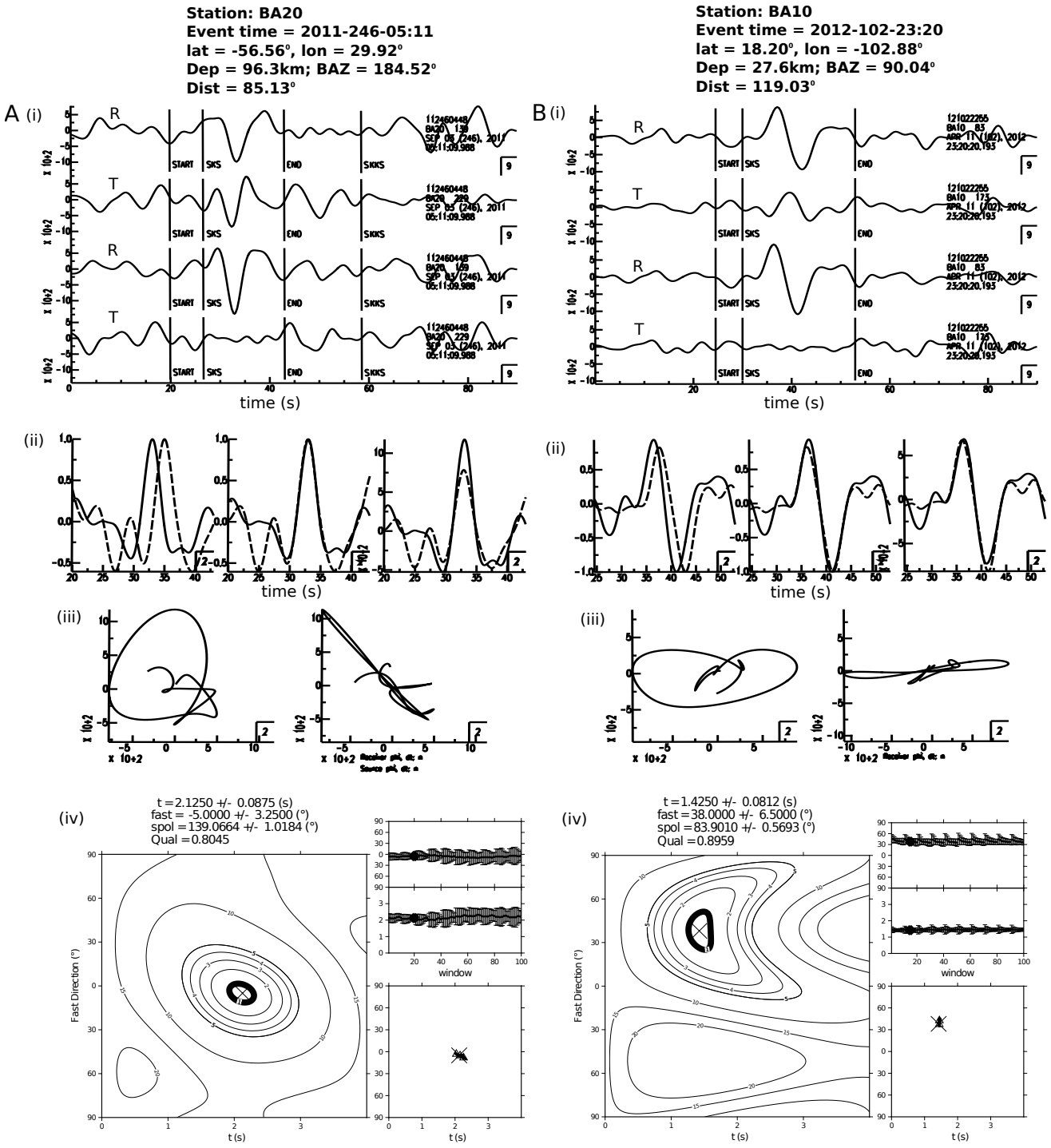

Fig. 5: Examples of shear wave splitting analyses for stations BA20 and BA10 which produce high quality split measurements. In each case (BA20(A) and BA10(B)): (i) radial and tangential components before (top) and after (bottom) correction by the splitting analysis; tangential SKS energy is minimized, (ii) windowed waveforms (dashed line: fast, solid line: slow) before and after correction applied; plot 2 is normalized and plot 3 shows the corrected waves with their relative amplitudes preserved, (iii) particle motion before and after correction, showing the change from elliptical to linearized motion, and (iv) grid search and cluster analysis outputs. The main graphic shows the final grid search results for ϕ and δt; the two smaller plots show individual measurements of ϕ and δt for the 100 windows used in the analysis.

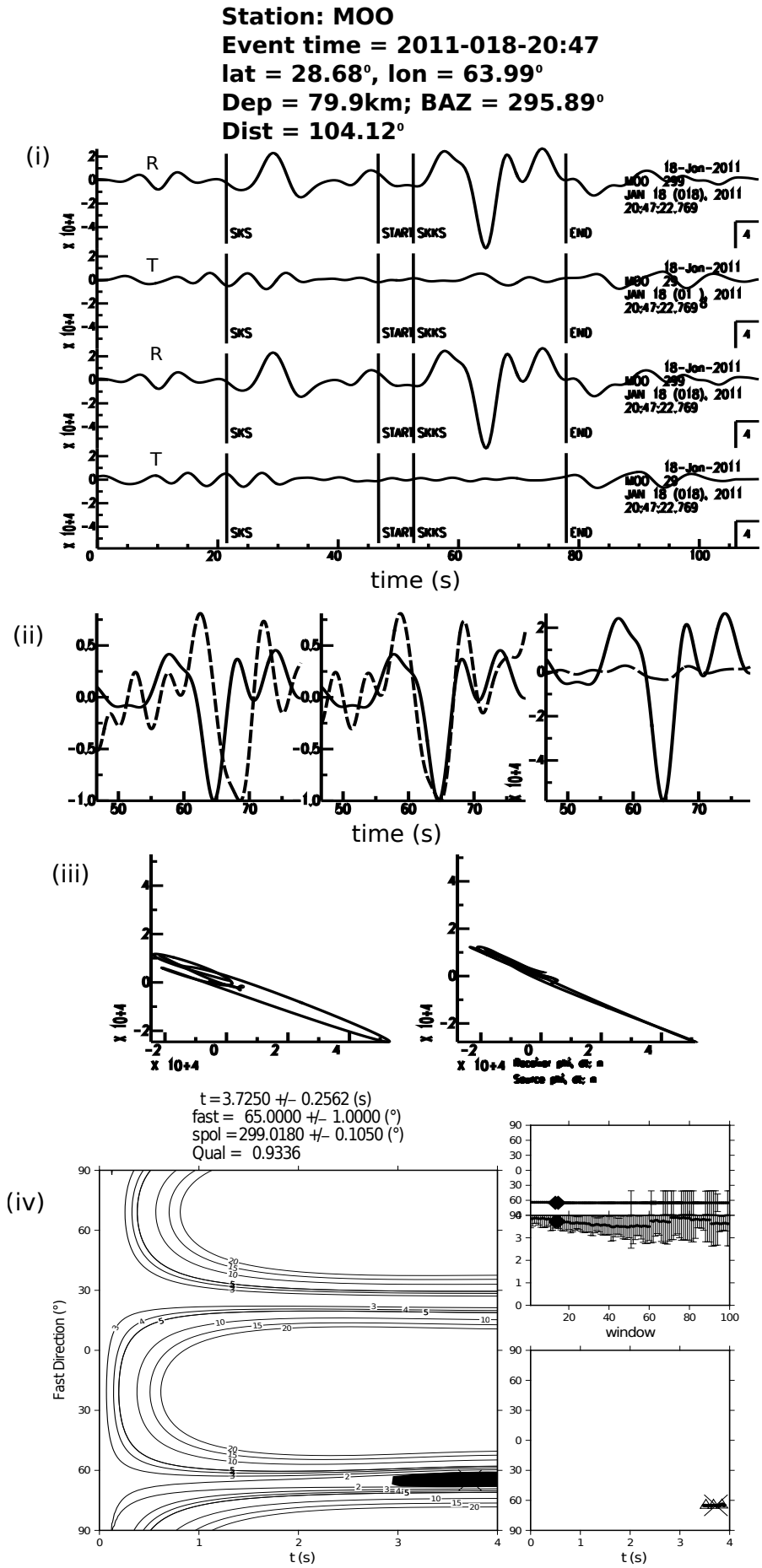

Fig. 6: A high-quality null. In this case, there is no signal on the tangential-component waveform, and the particle motion is linear both before and after analysis.

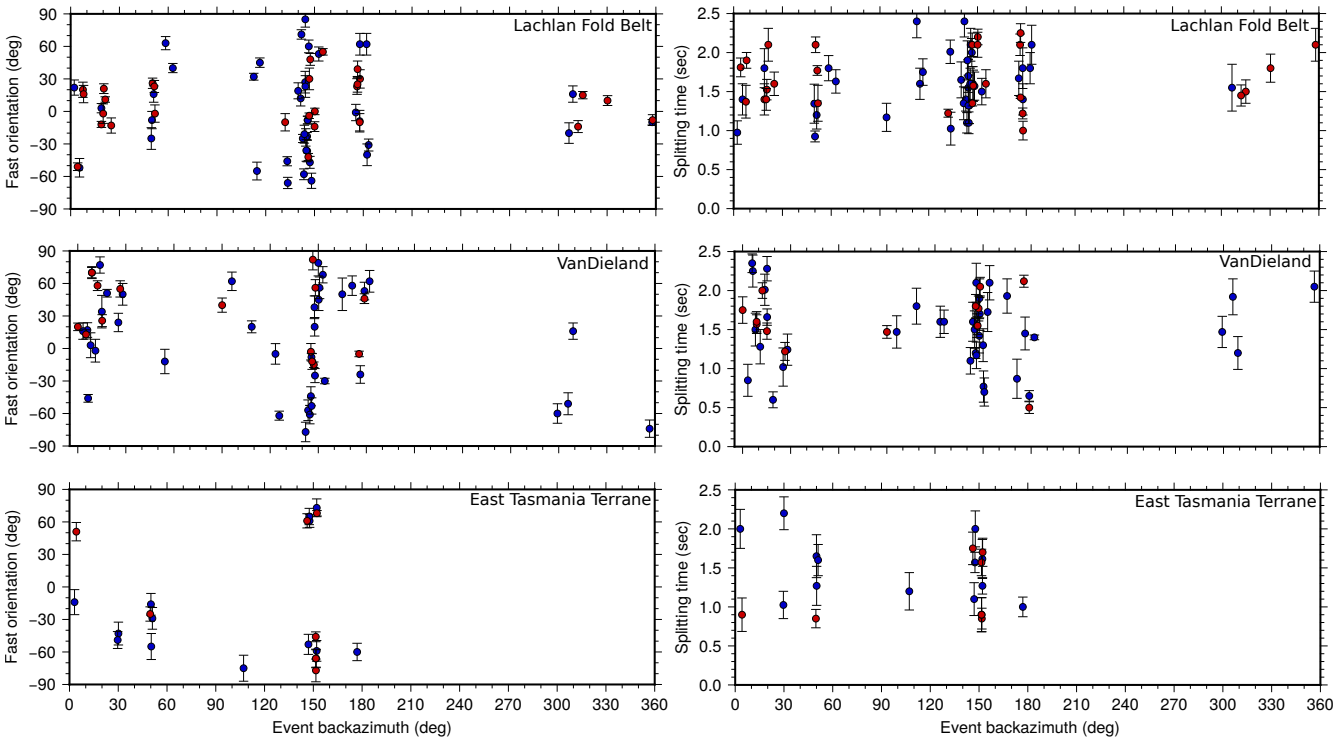

Fig. 7: Examples of the back azimuthal coverage of splitting results for the three tectonic blocks discussed in the text: Lachlan Fold Belt, VanDieland and East Tasmania Terrane + Furneaux Island. For each tectonic block, the left graph shows fast orientations and the right graph shows delay time; red represents good measurements, and blue represents fair measurements.

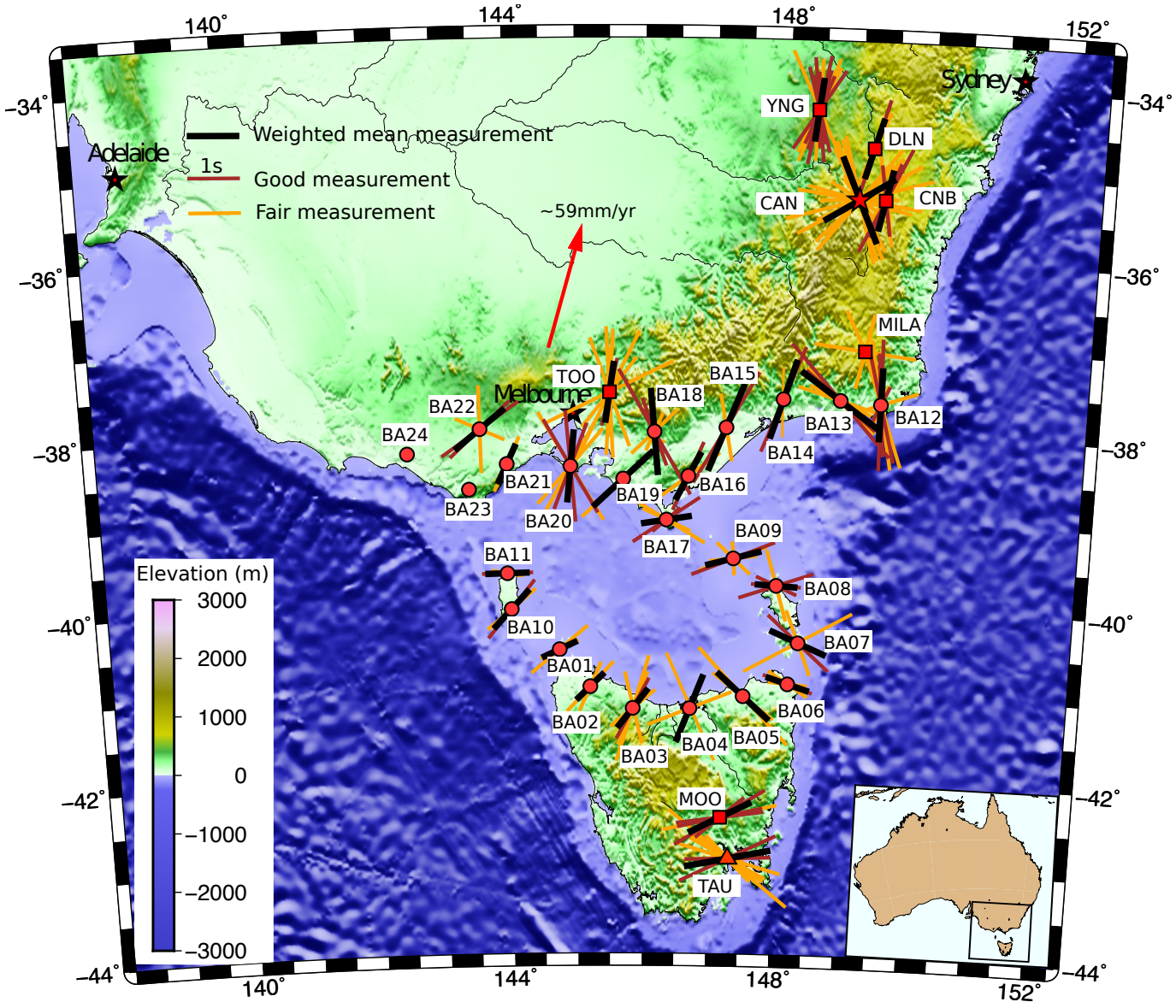

Fig. 8: Measured directions of polarization of the fast split shear wave. The length of each line is proportional to the delay time. Red arrow represents the APM direction calculated from NNR-MORVEL56 (Argus et al., 2011).

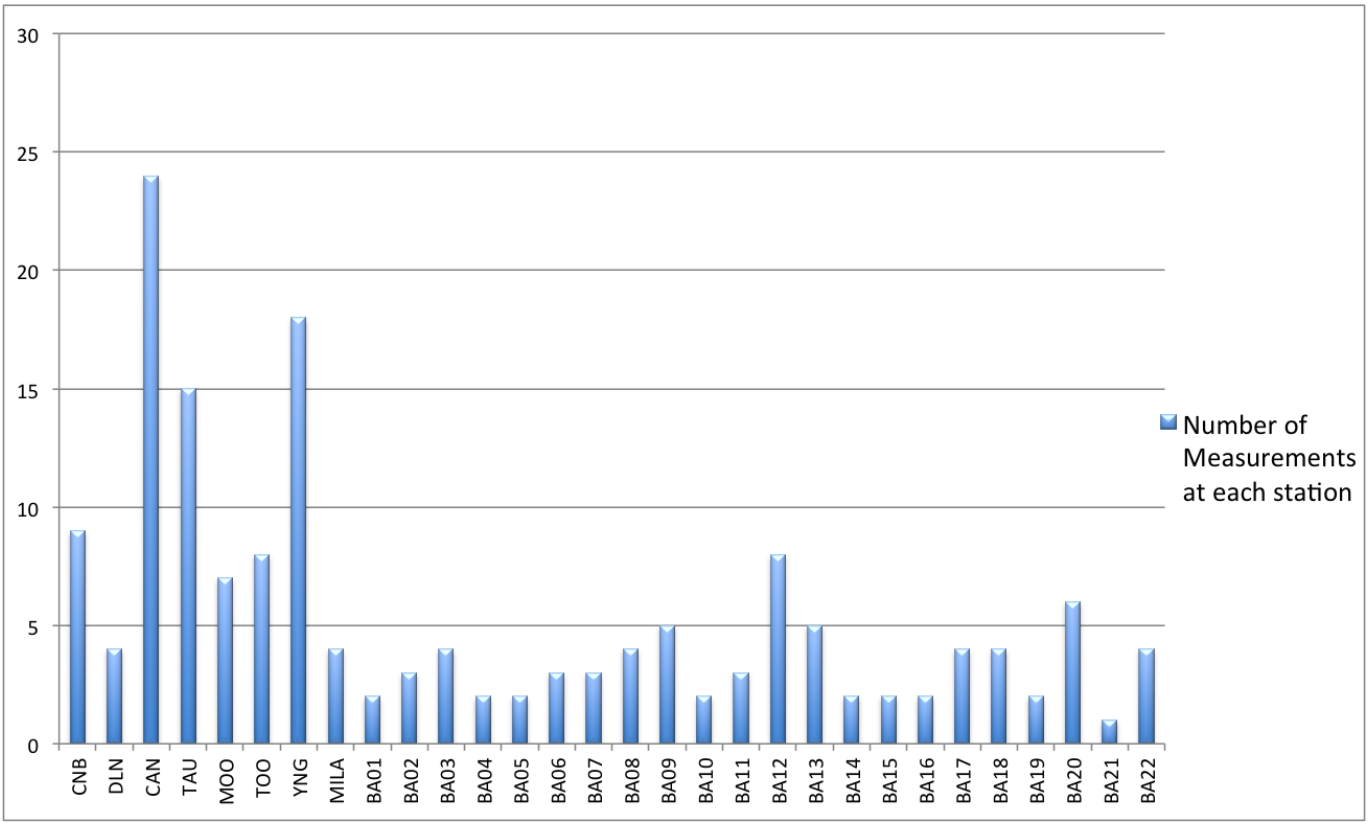

Fig. 9: A bar chart illustrating the number of measurements at individual stations.

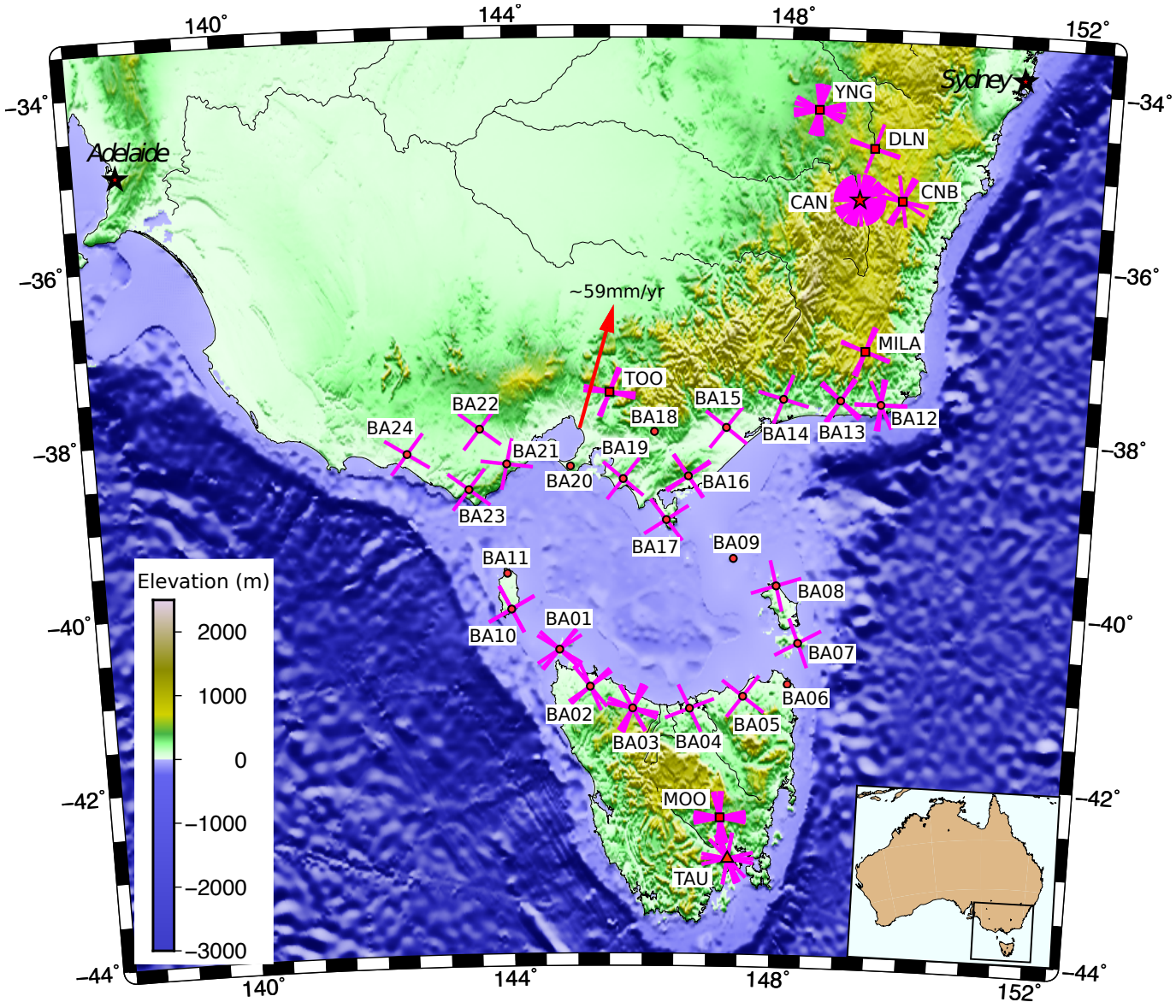

Fig. 10: Plot of null measurements for each station. The crosses denote absence of splitting: each branch is either parallel or perpendicular to a possible direction of anisotropy. Red arrow represents the APM direction calculated from NNR-MORVEL56 (Argus et al., 2011).

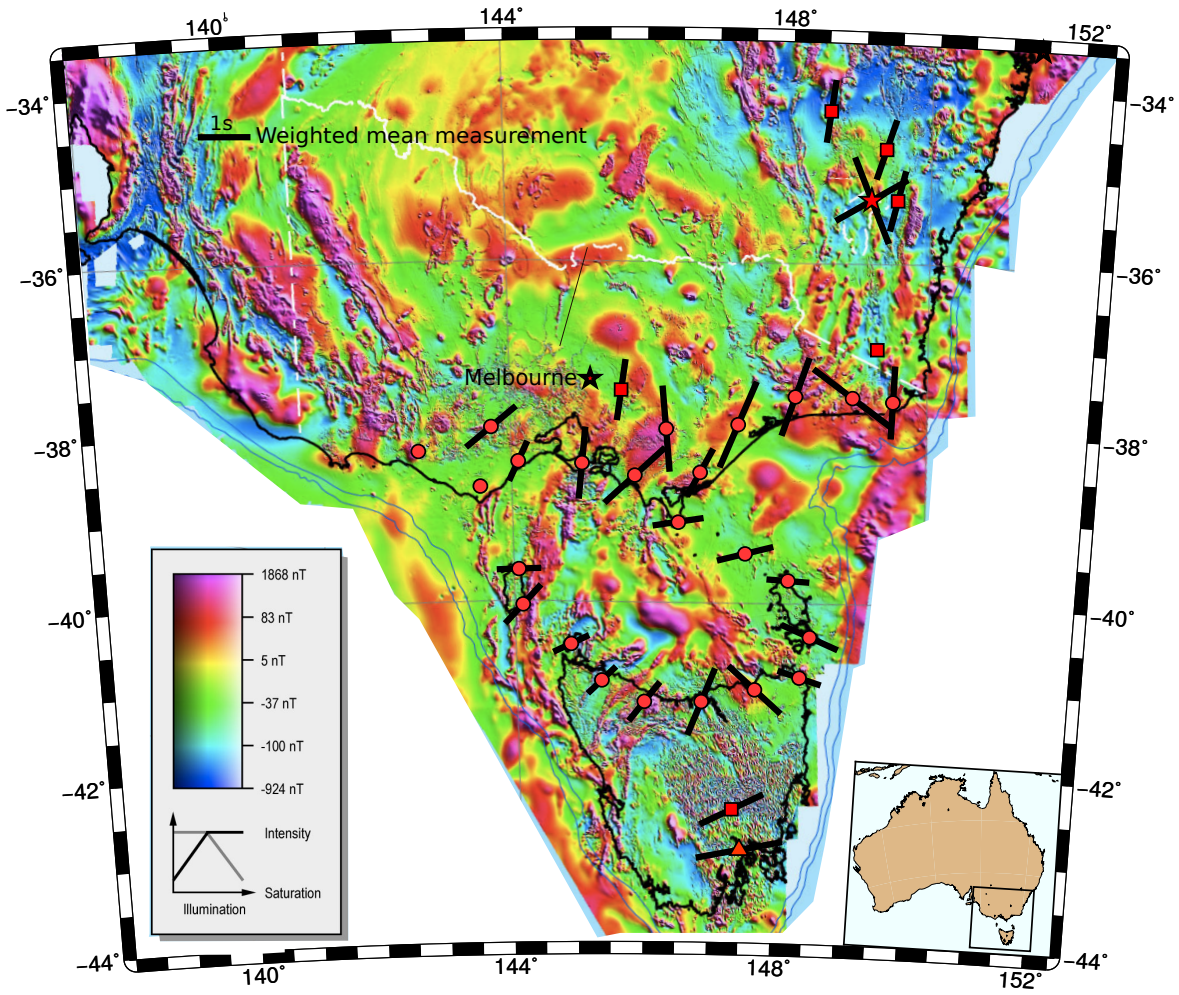

Fig. 11: Measured directions of polarization of the fast split shear wave superimposed on a magnetic anomaly map (modified from Milligan et al., 2010). The length of each line is proportional to the delay time.

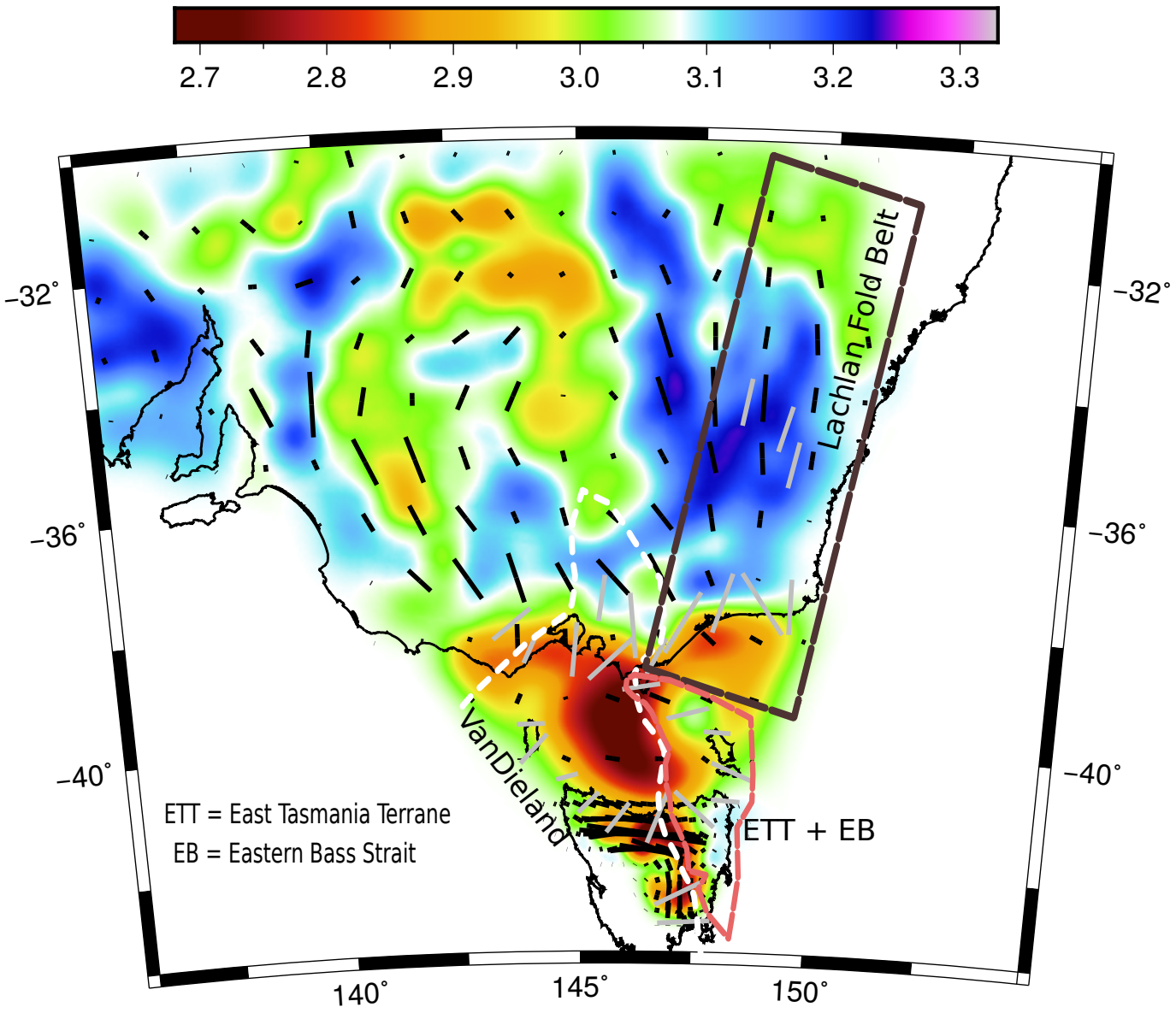

Fig. 12: Comparison of the new weighted mean SKS/SKKS splits (grey bars) superimposed on 5 second period Rayleigh wave phase anisotropy variations in the crust (black bars) (Pilia et al., 2016). For the Rayleigh wave phase anisotropy (black bars), the length of the bars is proportional to the magnitude of anisotropy, and the direction is aligned with the fast axis of anisotropy. The SKS/SKKS splits (grey bars) are scaled to 75% of the delay time magnitude for ease of comparison. The background colour represents the isotropic component of the 2D phase velocity map.

Table. 1: Weighted mean SKS/SKKS splitting parameters for each station. Quality assignments are given as: g = good; f = fair; and N = Null

Station	Lat. (°)	Long.(°)	Network	Total	Measurement categorisation	ϕ (weighted mean)		δt (weighted mean)	
						Upper (°)	Lower(°)	Upper(s)	Lower(s)
YNG	-34.298	148.396	ANSN	40	11g + 7f + 21N	7 ± 3		1.36 ± 0.07	
CNB	-35.315	149.363	ANSN	19	3g + 6f + 10N	13 ± 3		1.30 ± 0.14	
CAN	-35.319	148.996	GEOSCOPE	65	0g + 24f + 41N	58 ± 3	-23 ± 2	1.58 ± 0.15	1.78 ± 0.18
TAU	-42.909	147.320	GSN	36	3g + 12f + 21N	81 ± 9		1.34 ± 0.11	
MOO	-42.442	147.190	ANSN	23	5g + 2f + 16N	63 ± 3		1.33 ± 0.06	
TOO	-37.571	145.491	ANSN	18	1g +7f + 10N	08 ± 3		1.19 ± 0.16	
DLN	-34.723	149.179	ANSN	9	1g +3f + 5N	16 ± 2		1.22 ± 0.13	
BA01	-40.523	144.741	BASS	8	0g + 2f + 6N	65 ± 4		0.66 ± 0.10	
BA02	-40.950	145.200	BASS	7	1g + 2f + 4N	46 ± 2		0.75 ± 0.07	
BA03	-41.199	145.841	BASS	17	1g + 3f + 13N	38 ± 3		0.95 ± 0.04	
BA04	-41.196	146.704	BASS	4	0g +2f + 2N	21 ± 4		1.39 ± 0.19	
BA05	-41.050	147.506	BASS	5	0g +2f + 3N	-48 ± 3		1.35 ± 0.15	
BA06	-40.900	148.176	BASS	3	1g + 3f + 0N	-86 ± 3		0.73 ± 0.11	
BA07	-40.426	148.314	BASS	5	1g + 2f + 2N	-67 ± 4		1.17 ± 0.07	
BA08	-39.774	147.966	BASS	7	3g + 1f + 3N	-87 ± 2		0.68 ± 0.12	
BA09	-39.470	147.323	BASS	5	1g +4 f + 0N	75 ± 3		1.10 ± 0.03	
BA10	-40.056	144.030	BASS	7	1g + 1f + 5N	43 ± 1		1.03 ± 0.06	
BA11	-39.644	143.977	BASS	3	1g + 2f + 0N	89 ± 5		0.71 ± 0.13	
BA12	-37.662	149.412	BASS	14	4g + 4f + 6N	1 ± 2		1.41 ± 0.18	
BA13	-37.628	148.828	BASS	9	2g + 3f + 4N	-54 ± 2		1.87 ± 0.05	
BA14	-37.630	148.004	BASS	4	1g + 1f + 3N	18 ± 4		1.59 ± 0.14	
BA15	-37.967	147.186	BASS	4	1g + 1f + 2N	22 ± 3		1.79 ± 0.17	
BA16	-38.531	146.643	BASS	7	1g + 1f + 6N	28 ± 2		1.04 ± 0.12	
BA17	-39.035	146.327	BASS	6	2g + 2f + 2N	81 ± 6		0.98± 0.13	
BA18	-38.025	146.143	BASS	4	2g + 2f + 0N	-5 ± 4		1.68 ± 0.04	
BA19	-38.566	145.691	BASS	3	0g + 1f + 4N	47 ± 9		1.59 ± 0.18	
BA20	-38.420	144.920	BASS	6	3g + 3f + 0N	6 ± 2		1.40 ± 0.09	
BA21	-38.391	143.990	BASS	4	0g +1f + 3N	25 ± 9		1.15 ± 0.21	
BA22	-37.986	143.605	BASS	6	2g + 2f + 2N	51 ± 3		1.24 ± 0.16	